Case no.	Myocardial dysfunction	AVVR degree	Fetal treatment	GA at birth or death	Outcome	PMI
1	–	MR 1	–	36	Alive	–
2	–	TR 1	Beta	36	Alive	DDD→DDI
3	–	CAVVR 1	–	39	Alive	AAI
4	–	MR 2	–	37	Alive	–
5	–	–	–	37	Alive	–
6	–	CAVVR 2	Beta	37	Alive	VVI
7	–	CAVVR 2	–	37	Alive	DDI
8	–	–	–	38	Alive	DDD
9	–	CAVVR 2	Beta	37	Alive	AAI
10	+	TR 2	–	39	LD	DDD
11	+	TR 1	Beta	38	LD	DDD
12	+	CAVVR 2	Beta	31	LD	VVI
13	+	CAVVR 3	Beta	32	NND	DDD
14	+	CAVVR 2	Beta	36	NND	DDD
15	+	MR 2	Beta	35	NND	DDD
16	+	CAVVR 2	–	28	NND	–
17	+	–	Beta	32	FD	–
18	+	CAVVR 3	–	32	FD	–
19	+	–	–	21	FD	–
20	+	–	Beta	25	FD	–
21	–	CAVVR 2	–	39	LD	DDD
22	+	TR 2, MR 2	Beta	35	FD	–
23	–	–	–	39	Alive	VVI
24	–	–	–	38	Alive	–
25	–	MR 1	–	37	Alive	VVI
26	–	–	Beta	27	Alive	VVI
27	+	TR 2	–	37	Alive	VVI→DDD
28	–	TR 1	Beta	37	LD	VVI
29	+	–	–	36	NND	DDD

tion, of which 3 had fetal hydrops. Of the 22 cases of isomerism, 11 fetuses had a common atrioventricular canal, of which 9 had common atrioventricular valve regurgitation ≥2nd degree. In the 13 neonatal survivors with isomerism, 12 needed PMI; 4 underwent a total cavopulmonary connection at ages of 1.4, 1.6, 4.8, and 7.0 years, respectively, and 4 underwent functional repair. Of the 4 cases of corrected TGA, there were 2 of complete AVB without SSS, and 2 of second-degree AVB with and without SSS. None of the survivors of corrected TGA had fetal myocardial dysfunction or fetal hydrops; all survived, and 3 needed PMI. All 4 had PS (3 mild, 1 severe), and 3 had a ventricular septum defect, for which 2 underwent functional repair at 0.9 and 2.0 years old, respectively. Of the 3 with critical PS, all had complete AVB without SSS, and in 2 cases PMI was needed. All had duct-dependent pulmonary circulation. Of 2 cases of fetal myocardial dysfunction and fetal hydrops, one neonate died soon after birth with no response to resuscitation, and the other survived with functional repair through open pulmonary valvotomy at 5 days old.

Fetal Treatment

A β-sympathomimetic agent (continuous maternal infusion of ritodrine hydrochloride) was administered in utero in 13 cases, including 10 with left atrial isomerism, 1 with right atrial isomerism, 1 with corrected TGA, and 1 with critical PS. The ventricular heart rate increased by >10% in 6 cases (5 left atrial isomerism, 1 critical PS), and in 3 cases there was a temporary response. In the 6 responsive cases, 2 fetuses survived and 4 died after birth (1 in the neonatal period, 3 after the neonatal period). Of the 7 non-responsive cases, 2 fetuses survived and 5 died (3 in utero, 2 in the neonatal period). No fetus was treated with steroids or with an invasive intrauterine procedure such as PMI.

Risk Factors for All-Cause Mortality

The type of bradyarrhythmia was not associated with prognosis. All fetuses with a ventricular rate ≥70 beats/min survived. Kaplan-Meier survival curves for the primary endpoint of all-cause mortality showed that fetal hydrops, fetal myocardial dysfunction and a ventricular rate <55 beats/min (Figure 2) were significant risk factors for death (P<0.01, log-rank test). The results of univariate and multivariate Cox model analyses (Table 3) demonstrated that development of fetal myocardial dysfunction (hazard ratio [HR], 14.06; 95% confidence interval [CI]: 1.42–139.10, P=0.02), fetal hydrops (HR, 10.71; 95% CI: 1.15–100.00, P=0.04) and ventricular rate had significant effects on death (HR, 0.94; 95% CI: 0.88–1.00, P=0.04). A ventricular rate <55 beats/min had significant effects on fetal myocardial dysfunction (HR, 22.14; 95% CI: 1.60–306.79, P=0.02) and fetal hydrops (HR, 7.04; 95% CI: 1.14–43.58, P=0.04).

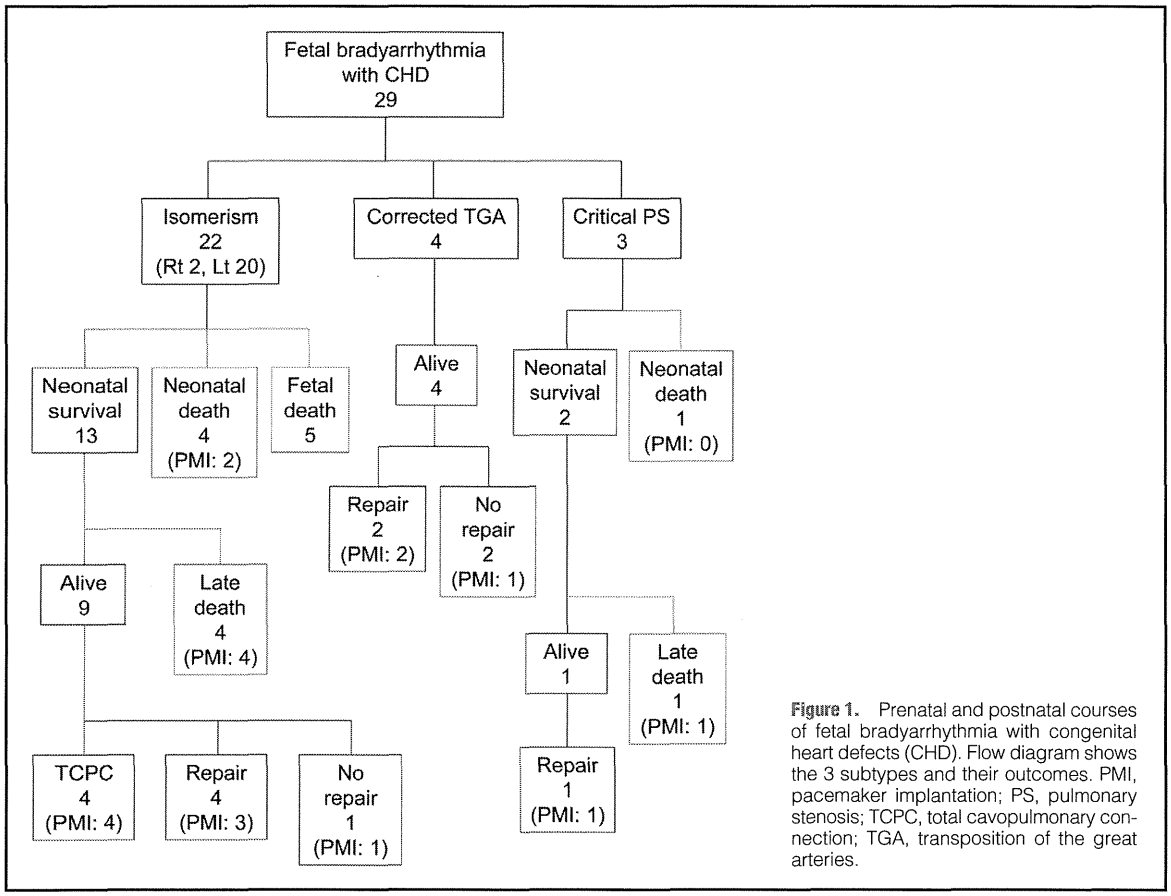

Figure 1. Prenatal and postnatal courses of fetal bradyarrhythmia with congenital heart defects (CHD). Flow diagram shows the 3 subtypes and their outcomes. PMI, pacemaker implantation; PS, pulmonary stenosis; TCPC, total cavopulmonary connection; TGA, transposition of the great arteries.

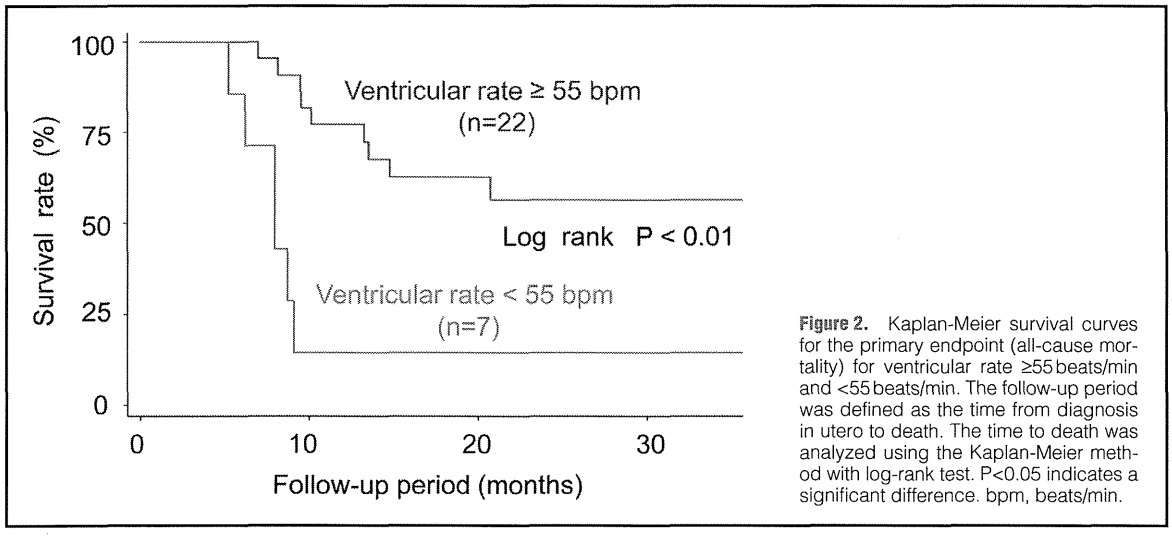

Figure 2. Kaplan-Meier survival curves for the primary endpoint (all-cause mortality) for ventricular rate ≥55 beats/min and <55 beats/min. The follow-up period was defined as the time from diagnosis in utero to death. The time to death was analyzed using the Kaplan-Meier method with log-rank test. P<0.05 indicates a significant difference. bpm, beats/min.

PMI in the Neonatal Period

There was a total of 12 cases of PMI in the neonatal period, of which 6 neonates survived and 6 died. Myocardial dysfunction tended to be more frequently associated in the cases of death than in survivors (100% vs. 33%, P=0.06). The mean ventricular rate at birth in the 2 groups was 61 beats/min. The pacing

Table 3. Predictors of Survival in Fetal Bradyarrhythmia With CHD

Variable	HR	95% CI	P value
Univariate			
GA at diagnosis	0.97	0.87–1.08	0.60
Ventricular rate at diagnosis	0.94	0.89–0.98	0.01
Atrial rate at diagnosis	0.99	0.97–1.02	0.63
Ventricular rate†	0.91	0.86–0.95	<0.01
Atrial rate‡	0.99	0.96–1.01	0.26
Development of bradycardia	3.21	1.14–9.04	0.03
Fetal hydrops at diagnosis	8.98	3.00–26.85	<0.01
Development of fetal hydrops	61.82	7.40–516.64	<0.01
Fetal myocardial dysfunction at diagnosis	18.75	4.04–86.93	<0.01
Development of fetal myocardial dysfunction	48.63	6.07–389.91	<0.01
AVVR	1.29	0.78–2.14	0.33
Fetal treatment	2.23	0.79–6.32	0.13
Effect of fetal treatment	1.21	0.38–3.82	0.75
Birth weight	1.00	1.00, 1.00	0.01
Ventricular rate at diagnosis <55 beats/min	3.45	0.96–12.42	0.06
Ventricular rate at diagnosis <65 beats/min	4.48	1.41–14.19	0.01
Ventricular rate <50 beats/min	25.26	4.61–138.42	<0.01
Ventricular rate <55 beats/min	5.49	1.86–16.21	<0.01
AVVR ≥2nd degree	0.36	0.08–1.60	0.18
Isomerism with a common atrioventricular canal	1.19	0.42–3.36	0.74
Multivariate			
Ventricular rate†	0.94	0.88–1.00	0.04
Development of fetal hydrops	10.71	1.15–100.00	0.04
Development of fetal myocardial dysfunction	14.06	1.42–139.10	0.02

P<0.05, significant difference. †Minimum ventricular heart rate recorded in utero; ‡minimum atrial heart rate recorded in utero. CI, confidence interval; HR, hazard ratio. Other abbreviation as in Tables 1,2.

rate was decided by the heart rate giving maximum systolic blood pressure, except in one case in which the pacing rate was blindly configured to 150 beats/min. The mean pacing rate was significantly higher in the cases of death than in survivors (133 beats/min vs. 107 beats/min, P=0.04).

Discussion

This study is one of the largest to investigate the prognosis and risk factors for fetal bradyarrhythmia associated with CHD. We found that the ventricular rate, type of CHD, myocardial dysfunction and fetal hydrops were important factors in predicting the outcome of fetuses with CHD. Fetuses with bradyarrhythmia associated with CHD had a worse prognosis than those without CHD, but our data also showed that those without risk factors had a relatively better clinical course. Hence, the outcome should not simply be predicted by the presence of CHD, but by associated factors in each case. For example, fetuses with corrected TGA and AVB had a good prognosis and those with ventricular heart rate ≥70 beats/min or good cardiac function had favorable outcomes. This is important information for clinicians and families in determining the appropriate management of affected fetuses.

A ventricular heart rate at diagnosis <55 beats/min had significant effects on fetal myocardial dysfunction and fetal hydrops, resulting in high mortality. Groves et al found that a ventricular heart rate <55 beats/min is a risk factor for fetal or neonatal death in fetuses with complete AVB without CHD,[19] but more recent multivariate analyses by Maeno et al and Jaeggi et al indicated that a ventricular heart rate <55 beats/min was not a risk factor.[20,21] Our previous study of fetal complete AVB without CHD also showed that the fetal ventricular heart rate was not associated with prognosis.[7] In contrast, our current study revealed that the ventricular heart rate was related to the outcome in fetuses with bradyarrhythmia with CHD. Jaeggi et al also found that a fetal heart rate <60 beats/min was not only associated with fetal hydrops, but predicted an adverse outcome in complete AVB with major CHD.[18] Thus, measurement of the ventricular heart rate is very important for predicting the outcome and prognosis of fetuses with bradyarrhythmia associated with CHD.

We found that the type of CHD was strongly associated with prognosis. Fetuses with corrected TGA and AVB had a good prognosis, as found in previous studies.[11–14] A poor prognosis of fetal bradyarrhythmia with CHD seems to be related to a high incidence of left isomerism.[15–20] The 5-year survival rates in all cases of left isomerism is low, ranging between 65% and 84%, even in recent studies, because of associated serious cardiac lesions.[22–25] High intrauterine mortality in cases of left atrial isomerism with complete AVB is often preceded by development of heart failure.[20,21] A high incidence of poor cardiac function and hydrops may partially explain the poor prognosis. We suggest that myocardial dysfunction could be ascribed to bradycardia and intrinsic ventricular dysfunction proceeding from the CHD.

Limited data are available on transplacental treatment of bradyarrhythmia associated with CHD. In a total of 10 cases of CHD such as left atrial isomerism, transplacental treatment was attempted using several types of β-sympathomimetics, but all but one died in utero or in the early neonatal peri-

od.[1,18,20,26] The fetal ventricular heart rate is increased by β-sympathomimetics in some cases, but a benefit of fetal treatment on survival has not been shown. Our retrospective multicenter study also did not demonstrate a significant benefit of the use of β-sympathomimetics on survival. This result can be partly explained by an obvious bias in this study because fetal treatment tended to be performed in severe cases of fetuses with a low heart rate and poor cardiac function (Table 2). However, it is very important to remember that long-term i.v. β-sympathomimetic treatment in mothers is reported to be associated with side-effects and may harm fetal cardiac function. Further accumulation of data is needed to clarify the beneficial and adverse effects of fetal treatment for this condition.

PMI is a crucial postnatal treatment in cases of fetal bradyarrhythmia. We did not find an effect of different modes of PMI, but a better outcome occurred with a slower heart rate setting. Previous reports in neonates with AVB without CHD showed improvement of cardiac function by reducing the pacing rate.[27,28] Thus, precise assessment of the appropriate setting for PMI may be required to optimize cardiac function, especially in cases of left isomerism with abnormal ventricular structure.

We found a relatively better prognosis than in studies performed outside Japan.[1,18,26,29] Although the follow-up period of 36±42 months was relatively short, the neonatal survival rate in our study was 48%, compared with only 14–18% in the previous studies. The type of arrhythmia comprised only complete AVB in the other studies, but we found the type of arrhythmia was not a risk factor for death in this study. Interestingly, another study from Japan (Maeno et al[20]) found similar outcomes to those in the current study. This result is partially explained by the low rates of termination of pregnancy in Japan. Furthermore, the other studies were performed 10–20 years ago and the improved outcomes may reflect the marked progress in neonatal treatment such as PMI and surgery.

Study Limitations

The main limitation to this study relate to retrospective data selection bias and the relatively small sample size. First, the nature of a multicenter retrospective observational study using a questionnaire is such that the clinical data obtained varied among cases. Clinical management during and after the fetal period also varied among centers. However, this was a strong dataset of current clinical courses because the response rate for the primary questionnaire exceeded 60% and data were gathered from tertiary pediatric cardiac centers and several regional perinatal institutions over a wide area of Japan. Second, the diagnosis of fetal myocardial dysfunction was made comprehensively and subjectively in different institutions, so we could not show the different variables of myocardial dysfunction based on the criterion of contraction, degree of cardiomegaly, or atrioventricular valve regurgitation. Because myocardial dysfunction included multiple findings, it might be more appropriate to use each finding rather than myocardial dysfunction as 1 variable for analysis. However, we considered it very important that this subjective finding made by the physicians who performed fetal echocardiography was related statistically to the outcome. Because one of the purposes of this study was to plan a future prospective study of managing fetal bradyarrhythmia with CHD, we decided to leave this subjective finding in order to emphasize in the future study the importance of objectively measuring cardiac function. Finally, termination of pregnancy is limited after 22 weeks of gestational age in Japan. Thus, some early and severe cases in which termination of pregnancy was performed may not have reached a regional perinatal center and would not have been identified by the questionnaire, resulting in the better outcomes in Japan. Nevertheless, we think that our results reflect more accurate outcomes of natural clinical courses compared with previous studies containing the selection bias of termination of pregnancy.

Conclusions

Neonatal and overall survival rates for fetal bradyarrhythmia with CHD were 66% and 48%, respectively. In fetal bradyarrhythmia with CHD, the type of associated CHD, fetal myocardial dysfunction, fetal hydrops, and ventricular rate were associated with a poor prognosis. Larger prospective studies are required to explore long-term morbidity and to establish appropriate treatment strategies for fetal bradyarrhythmia with CHD.

Acknowledgments

This work was supported by a grant from the Ministry of Health, Labour and Welfare of Japan (Health and Labour Science Research Grants for Clinical Research for New Medicine).

Disclosures

Competing Interests: None. Ethics Approval: Approved by the Institutional Review Board of the National Cerebral and Cardiovascular Center (M21-13).

References

1. Schmidt KG, Ulmer HE, Silverman NH, Kleinman CS, Copel JA. Perinatal outcome of fetal complete atrioventricular block: A multicenter experience. *J Am Coll Cardiol* 1991; **17:** 1360–1366.
2. Lopes LM, Tavares GM, Damiano AP, Lopes MA, Aiello VD, Schultz R, et al. Perinatal outcome of fetal atrioventricular block: One-hundred-sixteen cases from a single institution. *Circulation* 2008; **118:** 1268–1275.
3. Jaeggi ET, Fouron JC, Silverman ED, Ryan G, Smallhorn J, Hornberger LK. Transplacental fetal treatment improves the outcome of prenatally diagnosed complete atrioventricular block without structural heart disease. *Circulation* 2004; **110:** 1542–1548.
4. Eliasson H, Sonesson SE, Sharland G, Granath F, Simpson JM, Carvalho JS, et al. Isolated atrioventricular block in the fetus: A retrospective, multinational, multicenter study of 175 patients. *Circulation* 2011; **124:** 1919–1926.
5. Brucato A, Cimaz R, Caporaili R, Ramoni V, Buyon J. Pregnancy outcome in patients with autoimmune diseases and anti-Ro/SSA antibodies. *Clin Rev Allergy Immunol* 2011; **40:** 27–41.
6. Buyon JP, Ben-Chetrit E, Karp S, Roubey RA, Pompeo L, Reeves WH, et al. Acquired congenital heart block. Pattern of maternal antibody response to biochemically defined antigens of the SSA/Ro-SSB/La system in neonatal lupus. *J Clin Invest* 1989; **84:** 627–634.
7. Miyoshi T, Maeno Y, Sago H, Inamura N, Yasukohchi S, Kawataki M, et al. Evaluation of transplacental treatment for fetal congenital bradyarrhythmia: Nationwide survey in Japan. *Circ J* 2012; **76:** 469–476.
8. Ho SY, Fagg N, Anderson RH, Cook A, Allan L. Disposition of the atrioventricular conduction tissues in the heart with isomerism of the atrial appendages: Its relation to congenital complete heart block. *J Am Coll Cardiol* 1992; **20:** 904–910.
9. Anderson RH, Wenick ACG, Losekoot TG, Becker AE. Congenitally complete heart block-developmental aspects. *Circulation* 1977; **56:** 90–101.
10. Sharland G, Cook A. Heterotaxy syndromes/isomerism of the atrial appendages. *In*: Allan LD, Hornberger L, Sharland G, editors. Textbook of fetal cardiology. London: Greenwich Medical Media, 2000; 335–346.
11. Khairy P, Ionescu-Ittu R, Mackie AS, Abrahamowicz M, Pilote L, Marelli AJ. Changing mortality in congenital heart disease. *J Am Coll Cardiol* 2010; **56:** 1149–1157.
12. Marelli AJ, Mackie AS, Ionescu-Ittu R, Rahme E, Pilote L. Congenital heart disease in the general population: Changing prevalence and age distribution. *Circulation* 2007; **115:** 163–172.
13. Berg C, Geipel A, Smrcek J, Krapp M, Germer U, Kohl T, et al. Prenatal diagnosis of cardiosplenic syndromes: A 10-year experience. *Ultrasound Obstet Gynecol* 2003; **22:** 451–459.
14. Nagel B, Janousek J, Koestenberger M, Maier R, Sauseng W, Strenger

V, et al. Remote monitoring leads to early recognition and treatment of critical arrhythmias in adults after atrial switch operation for transposition of the great arteries. *Circ J* 2014; **78:** 450–456.
15. Lim JS, McCrindle BW, Smahorn JE, Golding F, Caldarone CA, Taketazu M, et al. Clinical features, management, and outcome of children with fetal and postnatal diagnoses of isomerism syndromes. *Circulation* 2005; **112:** 2454–2461.
16. Cuneo BF. Outcome of fetal cardiac defects. *Curr Opin Pediatr* 2006; **18:** 490–496.
17. Pepes S, Zidere V, Allan LD. Prenatal diagnosis of left atrial isomerism. *Heart* 2009; **95:** 1974–1977.
18. Jaeggi ET, Hornberger LK, Smallhorn JF, Fouron JC. Prenatal diagnosis of complete atrioventricular block associated with structural heart disease: Combined experience of two tertiary care centers and review of the literature. *Ultrasound Obstet Gynecol* 2005; **26:** 16–21.
19. Groves AMM, Allan LD, Rosenthal E. Outcome of isolated congenital complete heart block diagnosed in utero. *Heart* 1996; **75:** 190–194.
20. Maeno Y, Himeno W, Saito A, Hiraishi S, Hirose O, Ikuma M, et al. Clinical course of fetal congenital atrioventricular block in the Japanese population: A multicentre experience. *Heart* 2005; **91:** 1075–1079.
21. Jaeggi ET, Hamilton RM, Silverman ED, Zamora SA, Hornberger LK. Outcome of children with fetal, neonatal or childhood diagnosis of isolated congenital atrioventricular block. *J Am Coll Cardiol* 2002; **39:** 130–137.
22. Shiraishi I, Ichikawa H. Human heterotaxy syndrome: From molecular genetics to clinical features, management, and prognosis. *Circ J* 2012; **76:** 2066–2075.
23. Jacobs JP, Anderson RH, Weinberg PM, Walters HL 3rd, Tchervenkov CI, Del Duca D, et al. The nomenclature, definition and classification of cardiac structures in the setting of heterotaxy. *Cardiol Young* 2007; **17**(Suppl 2)**:** 1–28.
24. Cohen MS, Anderson RH, Cohen MI, Atz AM, Fogel M, Gruber PJ, et al. Controversies, genetics, diagnostic assessment, and outcomes relating to the heterotaxy syndrome. *Cardiol Young* 2007; **17**(Suppl 2)**:** 29–43.
25. Serraf A, Bensari N, Houyel L, Capderou A, Roussin R, Lebret E, et al. Surgical management of congenital heart defects associated with heterotaxy syndrome. *Eur J Cardiothorac Surg* 2010; **38:** 721–727.
26. Gembruch U, Hansmann M, Redel DA, Bald R, Knöpfle G. Fetal complete heart block: Antenatal diagnosis, significance and management. *Eur J Obstet Gynecol Reprod Biol* 1989; **31:** 9–22.
27. Silvetti MS, Drago F, Ravà L. Determinants of early dilated cardiomyopathy in neonates with congenital complete atrioventricular block. *Europace* 2010; **12:** 1316–1321.
28. Fang F, Sanderson JE, Yu CM. Potential role of biventricular pacing beyond advanced systolic heart failure. *Circ J* 2013; **77:** 1364–1369.
29. Machado MVL, Tynan MJ, Curry PVL, Allan LD. Fetal complete heart block. *Br Heart J* 1988; **60:** 512–515.

Gain-of-Function *KCNH2* Mutations in Patients with Brugada Syndrome

QI WANG, B.Sc.,* SEIKO OHNO, M.D., Ph.D.,* WEI-GUANG DING, M.D., Ph.D.,† MEGUMI FUKUYAMA, M.D.,* AKASHI MIYAMOTO, M.D., Ph.D.,* HIDEKI ITOH, M.D., Ph.D.,* TAKERU MAKIYAMA, M.D., Ph.D.,‡ JIE WU, Ph.D.,* JIAYU BAI, B.Sc.,† KANAE HASEGAWA, M.D.,* TETSUJI SHINOHARA, M.D., Ph.D.,§ NAOHIKO TAKAHASHI, M.D., Ph.D.,§ AKIHIKO SHIMIZU, M.D., Ph.D.,¶ HIROSHI MATSUURA, M.D, Ph.D.,† and MINORU HORIE, M.D., Ph.D.*

From the *Department of Cardiovascular and Respiratory Medicine, Shiga University of Medical Science, Otsu, Japan; †Division of Physiology, Shiga University of Medical Science, Otsu, Japan; ‡Department of Cardiovascular Medicine, Kyoto University Graduate School of Medicine, Kyoto, Japan; §Department of Cardiology and Clinical Examination, Oita University Faculty of Medicine, Yufu, Japan; and ¶Faculty of Health Sciences, Yamaguchi Graduate School of Medicine, Ube, Japan

Novel *KCNH2* Mutations in Brugada Syndrome. ***Background:*** **Brugada syndrome (BrS) is an inherited disease characterized by right precordial ST segment elevation on electrocardiograms (ECGs) that predisposes patients to sudden cardiac death as a result of polymorphic ventricular tachyarrhythmia or ventricular fibrillation (VF). In BrS patients, except for *SCN5A*, mutations in other responsible genes are poorly elucidated.**

Methods and Results: **We identified 4 *KCNH2* mutations, T152I, R164C, W927G, and R1135H, in 236 consecutive probands with BrS or Brugada-like ECG. Three of these mutation carriers showed QTc intervals shorter than 360 milliseconds and 1 experienced VF. We performed patch-clamp analyses on I_{Kr} reconstituted with the *KCNH2* mutations in Chinese hamster ovary cells and compared the phenotypes of the patients with different genotypes. Three mutations, R164C, W927G, and R1135H, increased I_{Kr} densities. Three mutations, T152I, R164C, and W927G, caused a negative shift in voltage-dependent activation curves. Only the R1135H mutant channel prolonged the deactivation time constants. We also identified 20 *SCN5A* and 5 *CACNA1C* mutation carriers in our cohort. Comparison of probands' phenotypes with 3 different genotypes revealed that *KCNH2* mutation carriers showed shorter QTc intervals and *SCN5A* mutation carriers had longer QRS durations.**

Conclusions: **All *KCNH2* mutations that we identified in probands with BrS exerted gain-of-function effects on I_{Kr} channels, which may partially explain the ECG findings in our patients.** *(J Cardiovasc Electrophysiol, Vol. 25, pp. 522-530, May 2014)*

Brugada syndrome, KCNH2, mutation, patch-clamp, ventricular tachycardia

Introduction

Brugada syndrome (BrS) is a hereditary disorder primarily caused by cardiac ion channel abnormality.[1] Ventricular fibrillation (VF) can occur without any structural heart disease in patients with BrS, leading to sudden cardiac death, particularly in apparently healthy young men.[2]

Recent studies[3,4] demonstrated that mutations in *SCN5A*, a gene encoding the α-subunit of the cardiac sodium channel, are the major cause of BrS. More than 300 *SCN5A* mutations are linked to BrS. However, *SCN5A* mutations account for only 18–30% of patients with BrS.[3] To date, more than 10 genes have been suspected to cause BrS[5,6]; however, mutations in these genes have been rarely identified in patients with BrS.[5,6]

KCNH2, or the human ether-a-go-go (hERG) gene, encodes an α-subunit of the rapid component of the delayed rectifier K^+ channel (Kv11.1). The Kv11.1 channel carries I_{Kr}, which plays an important role in regulating the repolarization of the cardiac action potential. Loss-of-function mutations of *KCNH2* are responsible for long-QT syndrome type 2. In 2005, 2 novel *KCNH2* mutations (G873S and N985S) were identified in patients with BrS who had no *SCN5A* mutation. Functional analyses of the 2 mutant channels and the computer simulation revealed that they caused gain-of-function of the Kv11.1 channel.[7] In 2009, we reported a novel *KCNH2* mutation, R1135H, in a patient showing a short-QT interval and Brugada electrocardiogram (ECG).[8] However, it remains unknown how these *KCNH2* mutations are associated with the clinical features.

Here, we conducted genetic testing on 9 BrS-associated genes and identified 4 *KCNH2* mutations (1.7%) in 236 consecutive probands with a BrS diagnosis or Brugada-like ECG. We have previously identified 20 *SCN5A* and 5 *CACNA1C* mutation carriers.[9] The functional outcomes of these *KCNH2*

This study was supported, in part by, a Grant-in-Aid for Scientific Research from the Japan Society for the Promotion of Science (KAKENHI) (to S.O. and M.H.) and by a Translational Research grant from the Japanese Circulation Society (to M.H.).

Address for correspondence: Seiko Ohno, M.D., Ph.D., Department of Cardiovascular and Respiratory Medicine, Shiga University of Medical Science, Otsu, Shiga 520-2192, Japan. Fax: +81-77-543-5839; E-mail: seikoono@kuhp.kyoto-u.ac.jp

Manuscript received 25 August 2013; Revised manuscript received 15 December 2013; Accepted for publication 23 December 2013.

doi: 10.1111/jce.12361

mutations were examined using a heterologous expression system. Finally, the clinical characteristics of the patients with *KCNH2* mutations were compared with the clinical characteristics of those with *SCN5A* or *CACNA1C* mutation.[9]

Methods

Study Population

The study population comprised 236 consecutive probands who were diagnosed with BrS or with Brugada-like ECG. They were enrolled at the Shiga University of Medical Science or the Kyoto University Graduate School of Medicine between 1996 and 2012 for genetic analyses. All study participants submitted written informed consent in accordance with the guidelines approved by each institutional review board.

Clinical Characteristics

We analyzed the following demographic characteristics: gender, age at diagnosis, history of symptoms (syncope, VF or sustained ventricular tachycardia [VT], and family history of sudden cardiac death). PR interval, QRS duration, and QT interval were manually measured in lead V_5, as shown on 12-lead ECG. QT intervals were corrected for the heart rate using Bazett's formula (QTc). According to the mode of Brugada pattern appearance, we classified its category[10] as (1) spontaneous, (2) upper precordial leads (3rd or 2nd intercostal position), or (3) after pure sodium channel blocker (pilsicainide) challenge test.

Genetic Analysis

Genomic DNA was isolated from leukocyte nuclei using a DNA extraction kit. We screened genetic variants of *KCNH2, SCN5A, GPD1L, CACNA1C, CACNB2, KCNE3, KCNE5, KCNJ8,* and *SCN1B* for all probands. In addition to these genes, we screened *SCN2B, SCN3B, SCN4B,* and *SCN10A* in patients with *KCNH2* mutation, who showed conduction block (PR interval $\geq$ 200 milliseconds). We used denaturing high-performance liquid chromatography (WAVE system Model 3500, Transgenomic, Omaha, NE, USA),[11-13] high-resolution melting,[14] and direct sequencing with the ABI PRISM-3130 sequencer (Applied Biosystems, Foster City, CA, USA) for the genetic analysis. The genetic analysis protocol was approved by the institutional ethics committees and was performed under its guidelines.

Mutagenesis and Transfection

We generated mutant constructs for the 3 novel *KCNH2* mutations. In brief, the human wild-type (WT) *KCNH2* cDNA was subcloned into the pRC-CMV vector. *KCNH2*-mutant plasmids were constructed using site-directed mutagenesis and a QuickChange-II-XL kit (Stratagene, La Jolla, CA, USA) and verified by DNA sequencing. Chinese hamster ovary (CHO) cells were cotransfected with 0.5 μg of pEGFP-N1/CMV and 1 μg WT or respective mutant *KCNH2* plasmid using lipofectamine and cultured at 37 °C, as reported previously.[8] Only green fluorescent protein-positive cells were used for the patch-clamp study.

Electrophysiological Study

The whole-cell configuration for patch-clamp recordings was conducted at 37 $\pm$ 1 °C using an EPC-8 patch-clamp amplifier 48–72 hours after transfection. The cells were superfused with a solution containing the following (in mmol/L): NaCl 140, KCl 5.4, CaCl 1.8, $MgCl_2$ 0.5, NaH_2PO_4 0.33, HEPES 5, and glucose 5.5 (pH 7.4 with NaOH). The pipette solution contained the following (in mmol/L): potassium aspartate 70, KCl 40, KH_2PO_4 10, EGTA 5, $MgSO_2$ 1, Na_2-ATP 3, Li-GTP 0.1, and HEPES 5 (pH 7.4 with KOH). Current density (pA/pF) was obtained by current amplitude divided by membrane capacitance (Cm) in each cell. Details of the experimental protocol are given in the legend of each figure.

Statistical Analysis

Continuous clinical data are expressed as mean $\pm$ standard deviation, and continuous patch-clamp data are expressed as mean $\pm$ standard error. Differences between continuous variables were evaluated using the independent Student's *t*-test for 2 groups, and one-way analysis of variance with Fisher's least significant difference test for 3 or more groups. Categorical values were evaluated by χ^2 test. A P value <0.05 was considered significant.

Results

Mutation Analysis

Four *KCNH2* mutations (3 novel mutations in this report) were identified in 236 consecutive probands (1.7%; Table 1). One of them was R1135H, which we previously reported with results of functional analysis.[8] These mutations were not observed in 512 control alleles from 206 healthy Japanese individuals and have not been reported according to the NHLBI Exome Sequencing Project, Exome Variant Server (http://evs.gs.washington.edu/EVS/), suggesting that the mutations are associated with the phenotype.

Two of the mutations resided in the N-terminus of Kv11.1 channel: (1) a C455T transition, causing a substitution of threonine with isoleucine at 152 (c. 455c > t; p. T152I; Fig. 1A), (2) a C-to-T transition, leading to the replacement of arginine at 164 by cysteine (c. 490c > t; p. R164C; Fig. 1B). The other 2 mutations were in the C-terminus: (3) a T-to-G transition, causing the substitution of tryptophan at codon 927 by glycine (c. 2799t > g; p. W927G; Fig. 1C), and (4) an A-to-G transition, leading to the replacement of arginine at 1135 by histidine (c. 3404a > g; p. R1135H; Fig. 1D).

The schematic topology in Figure 1E depicts locations of these mutations. Black star marks indicate the 2 mutations previously reported by Verkerk *et al.*[7] Interestingly, all the *KCNH2* mutations associated with BrS phenotypes are located in either N- or C-terminus.

Clinical Characteristics of the 4 KCNH2 Mutation Carriers

Table 1 summarizes the clinical characteristics of the 4 *KCNH2* mutation carriers.

Patient 1: The T152I mutation was identified in a 46-year-old man who consulted a doctor because of chest discomfort. Except for that, he had no other symptoms or

TABLE 1
Clinical Characteristic of *KCNH2* Mutation Carriers

Gene	Mutation	Age/Sex	BrS Type	VFVT	Syncope	FH	HR (bpm)	PR (milliseconds)	QRS (milliseconds)	QTc (milliseconds$^{1/2}$)
KCNH2	T152I	46/M	1[†]	–	–	–	59	180	70	386
KCNH2	R164C	56/M	1	–	–	+	57	200	80	342
KCNH2	W927G	32/M	1[‡]	+	+	–	51	150	80	350
KCNH2	R1135H	34/M	1	–	–	+	60	128	100	348

[†]BrS type 1 after sodium channel blocker. [‡]BrS type 1 at 3rd intercostal position.
FH = family history; HR = heart rate; M = male; VF = ventricular fibrillation; VT = ventricular tachycardia.

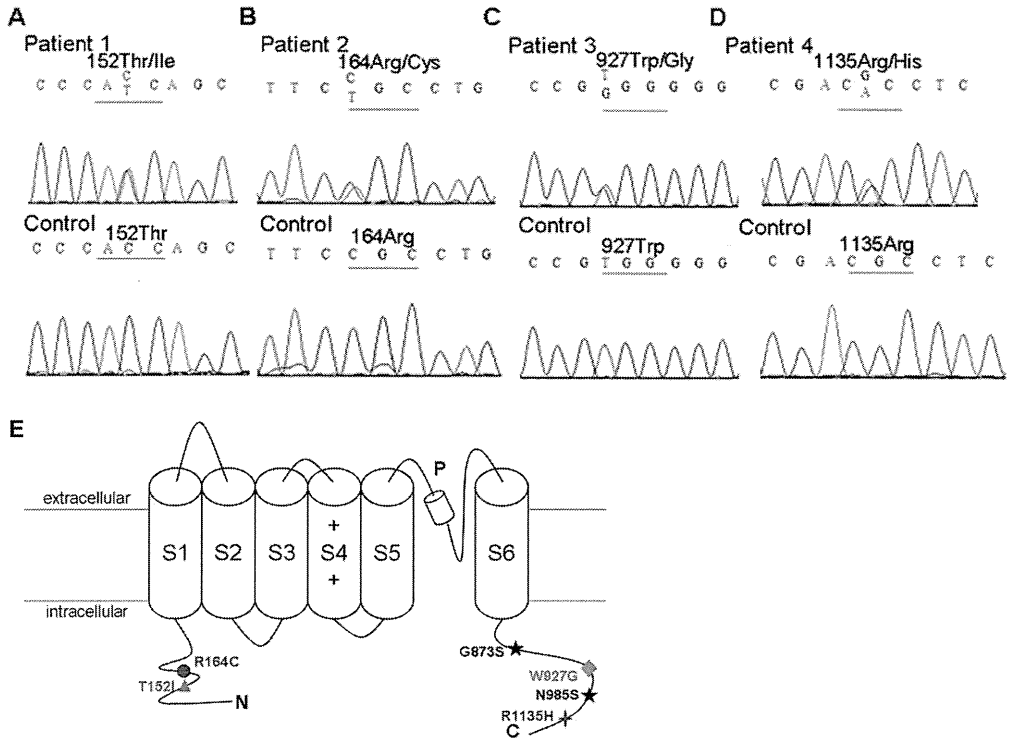

Figure 1. *Genetic analysis of KCNH2. A–D: DNA sequencing data in patients 1–4. A: Patient 1; c. 445c > t, p. T152I. B: Patient 2; c. 490c > t, p. R164C. C: Patient 3; c. 2799t > g, p. W927G. D: Patient 4; c. 3404a > g, p. R1135H. E: A schematic topology showing the Kv11.1 channel and locations of the KCNH2 mutations. Black star marks indicate the 2 mutations reported by Verkerk et al.*[7] *C = C-terminus; N = N-terminus; P = pore region; S1–S6 = transmembrane segments.*

family history of sudden cardiac death. His ECG showed type 2 Brugada ECG in the ordinary precordial positions, and an early repolarization pattern (~0.3 mV) was observed in the inferolateral leads (Fig. 2A). His heart rate, PR, QRS, and QTc intervals (QTc = 386 milliseconds$^{1/2}$) were normal. After the pilsicainide (50 mg, iv) challenge test, coved-type ST elevation was unmasked in V_1 and V_2 in the 3rd intercostal position.

Patient 2: The R164C mutation was identified in an asymptomatic 58-year-old man (indicated by the arrow in the pedigree of Fig. 2B) who was diagnosed with BrS because of coved-type ST elevation (Fig. 2B). His ECG also showed a relatively short QTc interval (QTc = 342 milliseconds$^{1/2}$). Although his father died from cerebral infarction, his maternal uncle had sudden cardiac death at the age of 55 years (pedigree in Fig. 2B). Because his ECG showed PR interval prolongation, we screened for *SCN2B-4B* and *SCN10A*; however, we did not identify any mutations in these genes. His mother was healthy without cardiac symptoms, though she refused cardiac examination and genetic analysis. Additional genetic data were not available for other family members.

Patient 3: A 32-year-old man carried the W927G mutation. He was working in the Japanese self-defense force. When he was moving on the highway for the mission, sitting in the front passenger's seat, he suddenly became unconscious after receiving a phone call in the car. Then VF was recognized by an automated external defibrillator. In his ECG, saddleback-type ST elevation in V_1 lead was recorded at the normal position, and it changed into coved-type at the 3rd intercostal position (Fig. 2C). His QTc interval was mildly shorter

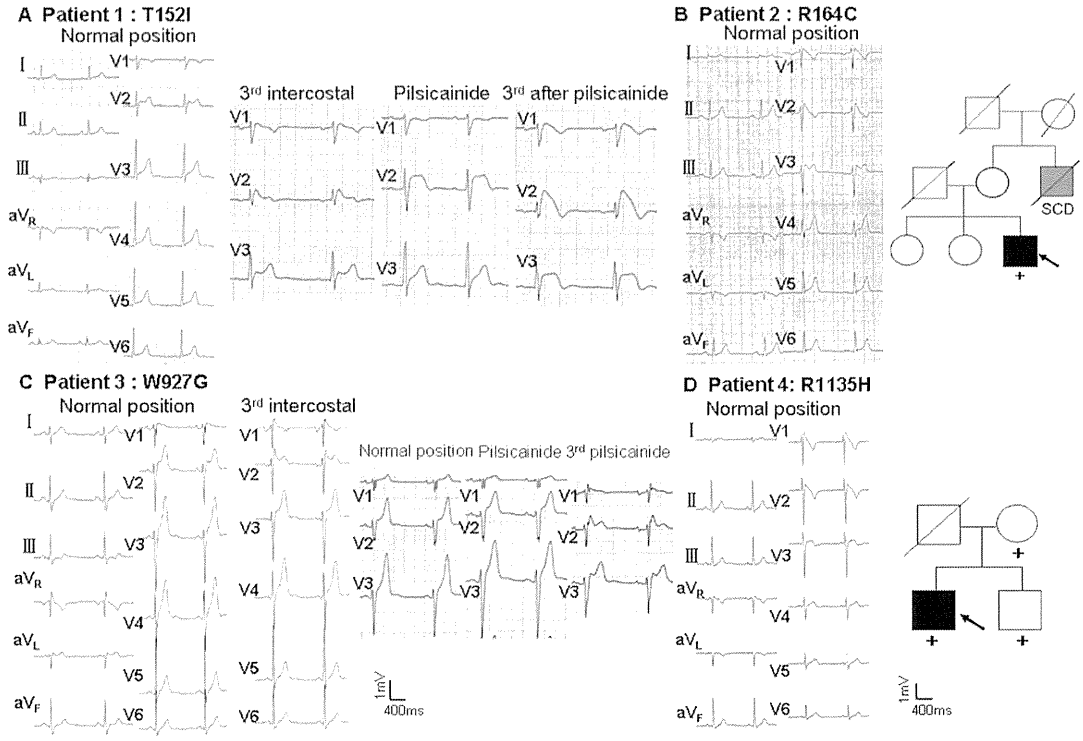

Figure 2. *Twelve-lead electrocardiograms (ECGs) in the 4 probands and pedigrees. A: ECGs of the T152I KCNH2 carrier before and after the pilisicainide challenge test recorded in the normal and 3rd precordial leads. Saddleback ST elevation was shown in the normal position. The saddleback ST elevation was changed to the coved-type on the 3rd intercostal recordings after the pilsicainide challenge test. B: ECG from patient 2, a 58-year-old man and his family tree. His ECG showed type 1 Brugada ECG in the right precordial leads and a shorter QTc interval (QTc = 346 milliseconds$^{1/2}$). His family tree is shown to the right of the ECG. C: Proband 3, a 32-year-old man who experienced ventricular fibrillation, showed a coved-type ST elevation in the 3rd intercostal position. The pilsicainide challenge test did not unmask coved-type ST segment. His QT interval was 350 milliseconds (QTc = 331 milliseconds$^{1/2}$). D: ECG from proband 4, a 34-year-old man and his family tree. We reported previously.[8] He had a type 1 Brugada ECG and shortening of the QT interval (QTc = 348 milliseconds$^{1/2}$). Arrow indicates the proband, black symbols indicate probands with BrS, gray symbol indicates a suspected patient with BrS, and plus mark indicates genotype positive.*

(350 milliseconds$^{1/2}$) than that of the normal range. According to the HRS/EHRA/APHRS consensus statement,[10] his ECG morphology and his symptoms could fulfill both BrS and short-QT syndrome. Therefore, we diagnosed him as overlapping BrS and short-QT syndrome. He received an implantable cardioverter defibrillator for the secondary prevention. He had no family history of sudden cardiac death. We failed to conduct genetic examination in his family members.

Patient 4: A 34-year-old man was admitted to the hospital under suspicion of BrS. His ECG (Fig. 2D) showed type 1 Brugada ECG as well as QTc shortening (QTc 348 milliseconds$^{1/2}$). This case was previously reported elsewhere.[8]

Functional Analysis of 4 Novel Mutant Kv11.1 Channels

Figure 3A shows 4 representative current traces recorded from CHO cells expressing *KCNH2*-WT and 3 *KCNH2* mutations (T152I, R164C, and W927G). Table 2 summarizes kinetics parameters obtained in the 5 different conditions. Time-dependent currents during test pulses increased with more depolarized voltage up to 0 mV and then decreased due to the inward rectification. Consequently, steady-state currents were maximal at around 0 mV, and the current–voltage (I–V) relationships showed a bell-shaped configuration (Fig. 3B). Current densities of mutant channels at the end of 2-second test potentials, except T152I, were significantly larger than those of the WT channel (Fig. 3B, Table 2, S-S). On the other hand, because the I–V relationship for the T1521 channel was significantly shifted to a more hyperpolarized direction (V_h: −26.9 mV vs. −19.0 mV in WT, Table 2, green symbols in Fig. 3B, C, and E), its current densities were larger than those of WT at test potentials between −60 and −30 mV.

Figure 3C depicts the relationships between peak tail current densities measured at −50 mV after various test potentials in the 5 different conditions. Peak tail current densities in 2 mutants (R164C and W927G indicated by solid circle and rhombus symbols) were significantly larger compared with those in WT. As we reported previously,[8] the R1135H mutant channel also showed larger tail current densities than those of WT (data not shown). In contrast, T152I channels carried significantly increased tail currents only after depolarization between −50 and −40 mV (Fig. 3C, triangle symbols).

In panel E of Figure 3, activation gates are shown after normalizing by peak tail current densities measured after the depolarization from +50 mV. Smooth lines were drawn

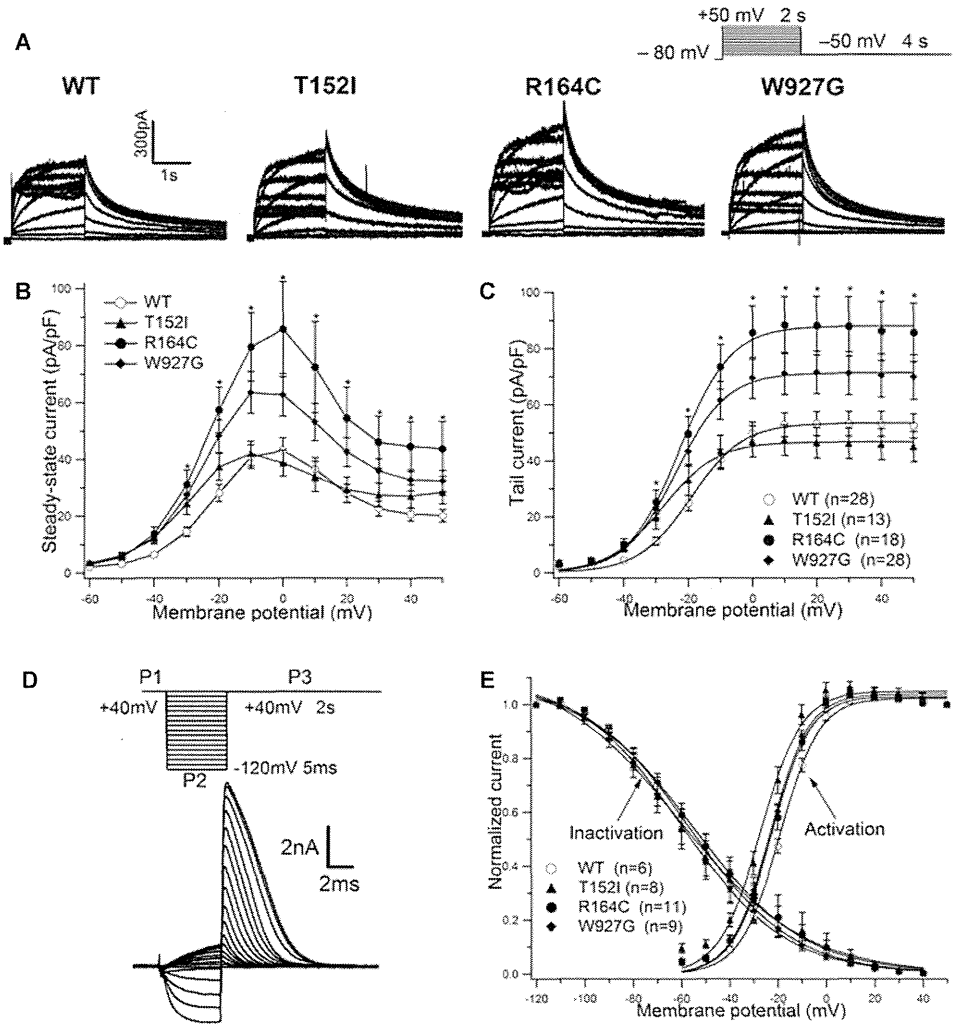

Figure 3. *Activation and inactivation kinetics of I_{Kr} currents reconstituted by wild type (WT) and 4 mutants. A: Representative current traces of WT and mutant-I_{Kr} (T152I, R164C, and W927G) expressed in CHO cells. The cells were held at −80 mV and given 2-second depolarization test pulses (between −50 and +50 mV) followed by a 4-second repolarization step to −50 mV (inset). E-4031 (1 μM)-sensitive currents are shown after digital subtraction of the 2 traces (baseline recoding, after inhibition by E-4031). B, C: Steady-state and tail current obtained from the experiments shown in (A). WT (hollow circle), T152I (solid triangle), R164C (solid circle), and W927G (solid rhombus). Each symbol indicates mean from multiple experiments (n > 10), and vertical bars indicate standard deviations. D: E-4031-sensitive currents elicited by the 3 voltage step protocol. At first, a depolarizing pulse of more than 1 second to +40 mV (P1) was applied, where current was activated and inactivated rapidly. Following this, a hyperpolarizing test pulse of 5 milliseconds was used for various potentials between −120 and +40 mV (P2) to allow rapid recovery from inactivation without producing significant deactivation, followed by a step to +40 mV (P3) (inset). E: Normalized activation and inactivation curves were fitted by the Boltzmann equation expressed as follows: $f(v) = I_{max}/(1 + \exp[(V_h - v)/k)]$, where v is the test voltage, I_{max} is the maximum current density of activation or inactivation, V_h is the half-maximum activation or inactivation voltage, and k is the slope factor.*

by fitting to the Boltzmann equation, and numeric data are listed in Table 2. Similarly to T152I, both R164C and W927G channels also produced a significant voltage shift to a more hyperpolarized direction.

Inset for Figure 3D shows the patch-clamp protocol to measure the steady-state voltage dependence of the inactivation gate and Figure 3D typical experimental results. Peak tail current densities recorded at P3 in multiple cells are plotted against test potentials (P2) in panel E. No significant differences were observed between the half-maximum inactivation voltages of mutant and WT channels.

Figure 4A depicts expanded current traces showing a very rapid recovery from inactivation on repolarization to various membrane potential applied as indicated in the inset. Its kinetic properties were estimated by fitting to a single exponential equation, as described in the figure legend. Time constants thus measured are plotted as a function of test potentials in Figure 4B, showing no significant differences between WT and the 3 mutant channels.

Figure 4C illustrates 4 representative current traces showing the I_{Kr} deactivation at various test potentials after depolarization to +40 mV. The decaying phases of tail currents

TABLE 2

Biophysical Kinetics of the 4 *KCNH2* Channels

		WT	T152I	R164C	W927G
Current densities (at 0 mV)	S-S (pA/pF)	43 ± 4.5	38.6 ± 4.6	85.7 ± 16.6*	62.6 ± 7.5*
	Tail (pA/pF)	49.7 ± 4.1	46.9 ± 5.5	85.6 ± 9.5*	69.8 ± 7.3*
Activation	V_h (mV)	−19.0 ± 0.9	−26.9 ± 1.6*	−22.5 ± 1.4*	−23.4 ± 0.9*
	k (mV)	7.8 ± 0.2	8.0 ± 0.5	7.3 ± 0.2	7.6 ± 0.3
Inactivation	V_h (mV)	−56.0 ± 3.9	−57.5 ± 8.8	−52.9 ± 5.2	−59.7 ± 4.7
	k (mV)	−20.5 ± 0.5	−20.1 ± 1.7	−20.1 ± 0.5	−20.2 ± 1.3
Recovery from inactivation (at −40 mV)	τ (milliseconds)	3.37 ± 0.32	2.82 ± 0.24	2.87 ± 0.18	3.21 ± 0.16
Deactivation	τ_{fast} (milliseconds)	623.5 ± 64.6	545.9 ± 124.4	649.2 ± 82.6	682.3 ± 95.6
	τ_{slow} (milliseconds)	5588.3 ± 505.3	5025.9 ± 1136.4	5425.8 ± 546.7	5732.7 ± 630.4

*$P < 0.05$ versus wild type (WT).
S-S = steady-state currents.

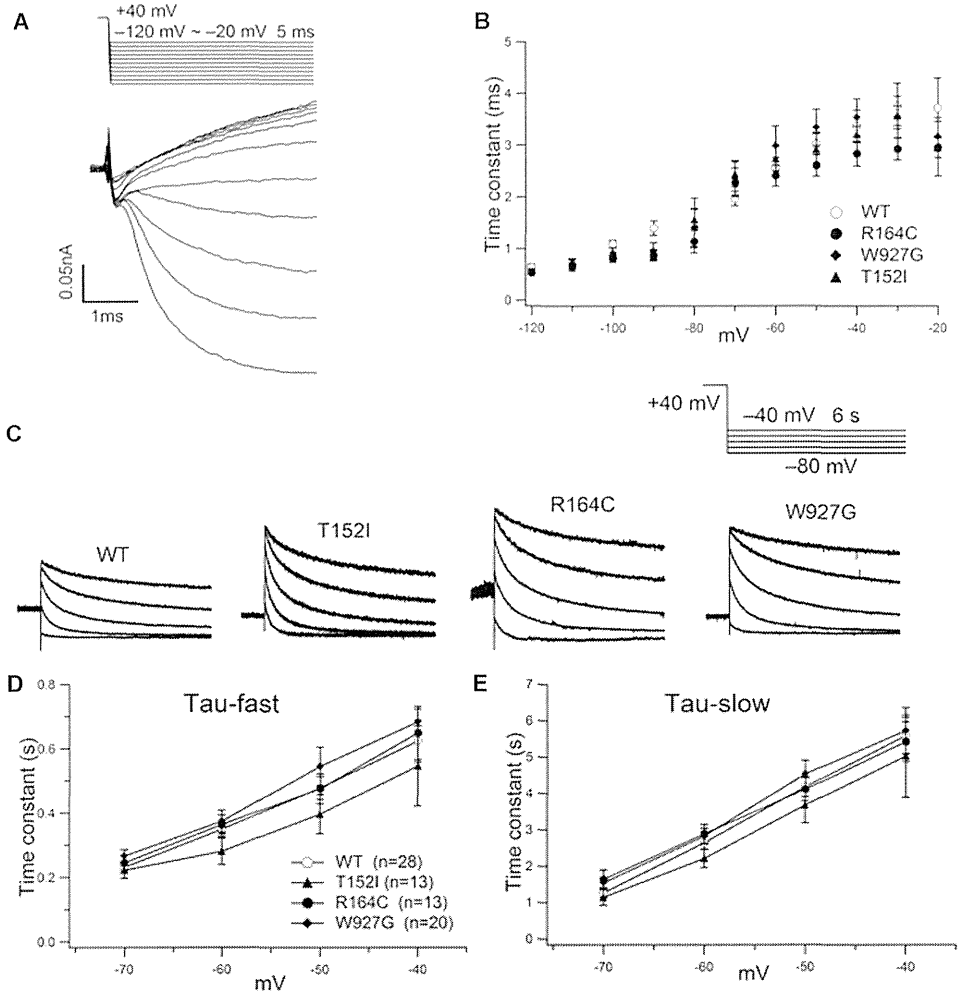

Figure 4. *Kinetic properties of recovery from inactivation and deactivation. A: Representative current traces showing recovery from inactivation. The recovery from I_{Kr} inactivation was measured from a holding potential of +40 mV to various test potentials between −120 and −20 mV (inset). Time constants (τ) of recovery from inactivation were obtained by fitting to a single exponential: $I_{Kr}(t) = A \cdot \exp(-t/\tau)$, where $I_{Kr}(t)$ is the current at time t, A is the maximum current amplitude. B: Time constants measured as in A are plotted as a function of the test potentials. C: Representative traces showing deactivation kinetics in the 5 different conditions. Decaying phases of tail currents elicited at various potentials (between −80 and −40 mV) for 6 seconds after a depolarizing prepulse to +40 mV (inset) were fitted to a double exponential equation: $I_{K,tail} = A_f \cdot \exp(-t/\tau_f) + A_s \cdot \exp(-t/\tau_s)$, where $I_{K,tail}$ were I_{Kr} currents of deactivation. A_f, A_s were decay phases of the currents. Fast (τ_f) (panel D) and slow (τ_s) (panel E) thus calculated are plotted against test potentials.*

TABLE 3
Summary and Comparison of Results in 3 Genotypes

	Total (n = 29)	*KCNH2* (n = 4)	*CACNA1C* (n = 5)	*SCN5A* (n = 20)	P Value
Male gender (%)	25 (86.2)	4 (100.0)	4 (80.0)	16 (85.0)	0.66
Age (years)	37 ± 19	42 ± 11	34 ± 13	37 ± 22	0.83
VF/VT (%)	8 (28.6)	1 (25.0)	1 (20.0)	6 (31.6)	0.87
Syncope (%)	12 (42.9)	1 (25.0)	1 (20.0)	10 (52.6)	0.31
Family history (%)	10 (35.7)	2 (50.0)	1 (20.0)	7 (36.8)	0.64
ECG measurements					
HR, bpm	68.8 ± 13.5	56.8 ± 4.0	68.4 ± 5.9	71.5 ± 14.9	0.14
PR interval, milliseconds	187.5 ± 36.6	164.5 ± 31.8	166.0 ± 35.8	198.1 ± 34.5	0.08
QRS duration, milliseconds	103.0 ± 17.6	77.5 ± 5.0*	91.2 ± 12.5*	111.5 ± 12.8	<0.0001
QTc interval, milliseconds$^{1/2}$	396.3 ± 31.3	356.5 ± 20.0	401.6 ± 19.9**	403.2 ± 30.0**	0.02

*P < 0.005 versus *SCN5A* group; **P < 0.05 versus *KCNH2* group.
Values are n, (%), or mean ± standard deviation.

could be fit to the sum of 2 exponential equations. Two time constants, Tau-fast and Tau-slow, were thus measured and are plotted against the test potentials in Figure 4D,E. No significant difference was observed in deactivation kinetics of the 3 other mutations compared with those of WT, although we reported a significantly slower deactivation in R1135H channels.[8]

Comparison of Clinical Characteristics Among the 3 Different Genotype Carriers

Collectively, our genetic analyses identified 4 *KCNH2* (their functional outcomes are described above), 5 *CACNA1C*, and 20 *SCN5A* mutations in total of 29 probands with BrS or Brugada-like ECG pattern. We compared the clinical features among these 3 genotypes (Table 3). Males were predominant (25 males, 86.2%), and this ratio was not significantly different among the 3 groups. Spontaneous VF and sustained VT were observed in 8 (28.6%) and syncope in 12 (42.9%). Ten (35.7%) had a family history of sudden cardiac death.

Ventricular arrhythmias were more associated with *SCN5A* mutation carriers (VF/VT, 31.6% and syncope, 52.6%), although it was not statistically significant. The resting heart rate and PR interval did not differ among the 3 groups. In contrast, QRS durations were significantly longer in the *SCN5A* group than in the other 2 groups, respectively (QRS duration: 111.5 ± 12.8 milliseconds vs. 77.5 ± 5.0 milliseconds and 91.2 ± 12.5 milliseconds, respectively, P < 0.0001). Compared with *SCN5A* and *CACNA1C* groups, QTc intervals were significantly shorter in *KCNH2* group (QTc intervals: 403.2 ± 30.0 milliseconds$^{1/2}$ and 401.6 ± 19.9 milliseconds$^{1/2}$ vs. 356.5 ± 20.0 milliseconds$^{1/2}$, respectively, P = 0.017).

Discussion

We identified 4 *KCNH2* mutations (3 novel and 1 previously reported; see Ref. 8) in 4 of 236 probands with BrS or Brugada-like ECG pattern. Biophysical analyses showed that all *KCNH2* mutations found in our cohort with BrS demonstrated gain-of-function effects to potentiate I_{Kr}.

Comparison with other 2 groups with BrS or Brugada-like ECG patterns of different genotypes; *SCN5A* and *CACNA1C*, we found that QT intervals were significantly shorter in *KCNH2* mutation group, and QRS durations were significantly longer in *SCN5A* mutation group (Table 3).

N588K was the first *KCNH2* mutation that was reported to have gain-of-function effects and responsible for short-QT syndrome[15] but not BrS. Brugada *et al.* identified this mutation in the S5-P loop region in 2 unrelated families with hereditary short-QT syndrome (QTc 300 milliseconds$^{1/2}$). Functional analyses of N588K channels revealed that it caused a complete loss of rectifying properties of Kv11.1 channels and did not inactive over the physiological range of potentials.[16]

In 2005, Verkerk *et al.*[7] first reported 2 *KCNH2* mutations (G873S and N985S) in cases with Brugada-like ECG pattern that modulated I_{Kr} properties: these 2 mutant channels showed increased I_{Kr} current densities. Then we found a mutation *KCNH2*-R1135H in a patient with Brugada ECG and short QTc interval. In a simulation study, Wilders and Verkerk[17] then demonstrated that the *KCNH2*-R1135H mutation not only shortened the action potential but also increased the susceptibility to all-or-none repolarization (loss-of-dome of action potentials in the right ventricle epicardium). Mutation-induced increase in I_{Kr} during initial activation may contribute to the premature repolarization, particularly in epicardium, a mechanism proposed for the BrS. This result suggests that, although not causative, these mutations may contribute to the Brugada phenotype in these families.

Similar to previous reports,[7,8] in this study we showed that 3 novel *KCNH2* mutations (T152I, R164C, and W927G) exerted gain-of-function effects on I_{Kr} channels without changing the inactivation kinetics. Clinical data confirmed that these 4 mutation (including R1135H we reported previously) carriers displayed BrS with or without relatively short-QT intervals. However, the mechanism underlying the gain-of-function of these novel mutations (T152I, R164C, and W927G) appeared quite different from that of N588K, in which the voltage dependence for inactivation was significantly shifted to more depolarized direction.

Although T152I and R164C reside in the N-terminus of Kv11.1, the current densities of R164C but not T152I were larger in both steady-state and tail currents than those of WT. The voltage-dependent activation profile of T152I and R164C channels was similar with a significant leftward shift (Fig. 3E). From the view of amino acid conformation, isoleucine (I) and threonine (T) are the only 2 amino acids that bear a chiral side chain (no change in nature of amino

acid residues in case of T152I), whereas cysteine (C) and arginine (R) have greatly different conformations and residual charge (R164C). These residual charges were supposedly the reason for the increased current densities in the R164C Kv11.1 channel.

As a β subunit of Kv11.1 channel, Mirp1 encoded by *KCNE2* has been reported, though its molecular correlation is still controversial.[18] We have no data of functional analysis in coexpression with mutant Kv11.1 and Mirp1. Therefore, our results may change under the condition with Mirp1.

As a genetic cause of BrS, we identified and analyzed *KCNH2* mutations in this study. Recently, however, Bezzina *et al.*[19] suggested that BrS may not be a monogenetic disorder, and some common genetic variants may have strong modifier effects. Although we showed gain-of-functions in mutant I_{Kr} channels in our study, we cannot conclude that the mutations are the only cause of the disease as previous study suggested.[7] And other rare or common variants may together conduct to cause the disease; in other words, our mutations can be modifiers of BrS.

Compared to *KCNH2* and *CACNA1C* mutation carriers, *SCN5A* mutation carriers had longer QRS intervals (Table 3), suggesting that some *SCN5A* mutations are associated not only with BrS but also with conduction block.[20-23] Patients with *SCN5A*-linked BrS had a higher prevalence of bradyarrhythmia than non-*SCN5A*-linked BrS patients.[4] Therefore, distinguished from *KCNH2* mutations, the loss-of-function type *SCN5A* mutations, either by altering gating kinetics[21,23] or by attenuating trafficking properties,[23] may cause conduction deficiency. The high frequency of syncope among *SCN5A* mutation carriers in our study (52.6%, Table 3) may be related, although the frequency of syncope was not significantly different among groups. Because QTc interval in 3 of 4 *KCNH2* mutation carriers was relatively shorter than 360 milliseconds[1/2], that led to shortening the average QTc value in the clinical comparison.

Study Limitation

We performed functional analysis in only homozygous expression types. Therefore, the results may not mimic the phenotypes of the patients with heterozygous mutations.

Conclusions

We identified 4 *KCNH2* mutations (3 novel and 1 previously reported; see Ref. 8) in BrS patients. All mutations functionally increased I_{Kr}, suggesting their correlation with the phenotypes.

Acknowledgment: We are grateful to Ms. A. Ikeda and Ms. A. Umehara for their technical assistance.

References

1. Brugada P, Brugada J: Right bundle branch block, persistent ST segment elevation and sudden cardiac death: A distinct clinical and electrocardiographic syndrome. A multicenter report. J Am Coll Cardiol 1992;20:1391-1396.
2. Benito B, Sarkozy A, Mont L, Henkens S, Berruezo A, Tamborero D, Arzamendi D, Berne P, Brugada R, Brugada P, Brugada J: Gender differences in clinical manifestations of Brugada syndrome. J Am Coll Cardiol 2008;52:1567-1573.
3. Antzelevitch C, Brugada P, Borggrefe M, Brugada J, Brugada R, Corrado D, Gussak I, LeMarec H, Nademanee K, Perez Riera AR, Shimizu W, Schulze-Bahr E, Tan H, Wilde A: Brugada syndrome: Report of the second consensus conference: Endorsed by the Heart Rhythm Society and the European Heart Rhythm Association. Circulation 2005;111:659-670.
4. Makiyama T, Akao M, Tsuji K, Doi T, Ohno S, Takenaka K, Kobori A, Ninomiya T, Yoshida H, Takano M, Makita N, Yanagisawa F, Higashi Y, Takeyama Y, Kita T, Horie M: High risk for bradyarrhythmic complications in patients with Brugada Syndrome caused by SCN5A gene mutations. J Am Coll Cardiol 2005;46:2100-2106.
5. Mizusawa Y, Wilde AA: Brugada syndrome. Circ Arrhythm Electrophysiol 2012;5:606-616.
6. Crotti L, Marcou CA, Tester DJ, Castelletti S, Giudicessi JR, Torchio M, Medeiros-Domingo A, Simone S, Will ML, Dagradi F, Schwartz PJ, Ackerman MJ: Spectrum and prevalence of mutations involving BrS1-through BrS12-susceptibility genes in a cohort of unrelated patients referred for Brugada syndrome genetic testing: Implications for genetic testing. J Am Coll Cardiol 2012;60:1410-1418.
7. Verkerk AO, Wilders R, Schulze-Bahr E, Beekman L, Bhuiyan ZA, Bertrand J, Eckardt L, Lin D, Borggrefe M, Breithardt G, Mannens MM, Tan HL, Wilde AA, Bezzina CR: Role of sequence variations in the human ether-a-go-go-related gene (hERG, KCNH2) in the Brugada syndrome. Cardiovasc Res 2005;68:441-453.
8. Itoh H, Sakaguchi T, Ashihara T, Ding WG, Nagaoka I, Oka Y, Nakazawa Y, Yao T, Jo H, Ito M, Nakamura K, Ohe T, Matsuura H, Horie M: A novel KCNH2 mutation as a modifier for short QT interval. Int J Cardiol 2009;137:83-85.
9. Fukuyama M, Ohno S, Wang Q, Kimura H, Makiyama T, Itoh H, Ito M, Horie M: L-type calcium channel mutations in Japanese patients with inherited arrhythmias. Circ J 2013;77:1799-1806.
10. Priori SG, Wilde AA, Horie M, Cho Y, Behr ER, Berul C, Blom N, Brugada J, Chiang CE, Huikuri H, Kannankeril P, Krahn A, Leenhardt A, Moss A, Schwartz PJ, Shimizu W, Tomaselli G, Tracy C: HRS/EHRA/APHRS expert consensus statement on the diagnosis and management of patients with inherited primary arrhythmia syndromes: Expert consensus statement on inherited primary arrhythmia syndromes: Document endorsed by HRS, EHRA, and APHRS in may 2013 and by ACCF, AHA, PACES, and AEPC in June 2013. Heart Rhythm 2013:e75-e106.
11. Itoh H, Shimizu W, Hayashi K, Yamagata K, Sakaguchi T, Ohno S, Makiyama T, Akao M, Ai T, Noda T, Miyazaki A, Miyamoto Y, Yamagishi M, Kamakura S, Horie M: Long QT syndrome with compound mutations is associated with a more severe phenotype: A Japanese multicenter study. Heart Rhythm 2010;7:1411-1418.
12. Ohno S, Zankov DP, Yoshida H, Tsuji K, Makiyama T, Itoh H, Akao M, Hancox JC, Kita T, Horie M: N- and C-terminal KCNE1 mutations cause distinct phenotypes of long QT syndrome. Heart Rhythm 2007;4:332-340.
13. Jongbloed R, Marcelis C, Velter C, Doevendans P, Geraedts J, Smeets H: DHPLC analysis of potassium ion channel genes in congenital long QT syndrome. Hum Mutat 2002;20:382-391.
14. Millat G, Chanavat V, Créhalet H, Rousson R: Development of a high resolution melting method for the detection of genetic variations in long QT syndrome. Clin Chim Acta 2011;412:203-207.
15. Brugada R, Hong K, Dumaine R, Cordeiro J, Gaita F, Borggrefe M, Menendez TM, Brugada J, Pollevick GD, Wolpert C, Burashnikov E, Matsuo K, Wu YS, Guerchicoff A, Bianchi F, Giustetto C, Schimpf R, Brugada P, Antzelevitch C: Sudden death associated with short-QT syndrome linked to mutations in hERG. Circulation 2004;109:30-35.
16. Grunnet M, Diness TG, Hansen RS, Olesen SP: Biophysical characterization of the short QT mutation hERG-N588K reveals a mixed gain-and loss-of-function. Cell Physiol Biochem 2008;22:611-624.
17. Wilders R, Verkerk AO: Role of the R1135H KCNH2 mutation in Brugada syndrome. Int J Cardiol 2010;144:149-151.
18. Eldstrom J, Fedida D: The voltage-gated channel accessory protein KCNE2: Multiple ion channel partners, multiple ways to long QT syndrome. Expert Rev Mol Med 2011;13:e38.
19. Bezzina CR, Barc J, Mizusawa Y, Remme CA, Gourraud JB, Simonet F, Verkerk AO, Schwartz PJ, Crotti L, Dagradi F, Guicheney P, Fressart V, Leenhardt A, Antzelevitch C, Bartkowiak S, Schulze-Bahr E, Zumhagen S, Behr ER, Bastiaenen R, Tfelt-Hansen J, Olesen MS, Kääb S, Beckmann BM, Weeke P, Watanabe H, Endo N, Minamino T, Horie M, Ohno S, Hasegawa K, Makita N, Nogami A, Shimizu W, Aiba T, Froguel P, Balkau B, Lantieri O, Torchio M, Wiese C, Weber D,

Wolswinkel R, Coronel R, Boukens BJ, Bézieau S, Charpentier E, Chatel S, Despres A, Gros F, Kyndt F, Lecointe S, Lindenbaum P, Portero V, Violleau J, Gessler M, Tan HL, Roden DM, Christoffels VM, Le Marec H, Wilde AA, Probst V, Schott JJ, Dina C, Redon R: Common variants at SCN5A-SCN10A and HEY2 are associated with Brugada syndrome, a rare disease with high risk of sudden cardiac death. Nat Genet 2013;45:1044-1049.

20. Kyndt F, Probst V, Potet F, Demolombe S, Chevallier JC, Baro I, Moisan JP, Boisseau P, Schott JJ, Escande D, Le Marec H: Novel SCN5A mutation leading either to isolated cardiac conduction defect or Brugada syndrome in a large French family. Circulation 2001;104:3081-3086.
21. Tan HL, Bink-Boelkens MT, Bezzina CR, Viswanathan PC, Beaufort-Krol GC, van Tintelen PJ, van den Berg MP, Wilde AA, Balser JR: A sodium-channel mutation causes isolated cardiac conduction disease. Nature 2001;409:1043-1047.
22. Schott JJ, Alshinawi C, Kyndt F, Probst V, Hoorntje TM, Hulsbeek M, Wilde AA, Escande D, Mannens MM, Le Marec H: Cardiac conduction defects associate with mutations in SCN5A. Nat Genet 1999;23:20-21.
23. Tan BH, Iturralde-Torres P, Medeiros-Domingo A, Nava S, Tester DJ, Valdivia CR, Tusie-Luna T, Ackerman MJ, Makielski JC: A novel C-terminal truncation SCN5A mutation from a patient with sick sinus syndrome, conduction disorder and ventricular tachycardia. Cardiovasc Res 2007;76:409-417.

ARTICLE IN PRESS
LFS-14192; No of Pages 8
Life Sciences xxx (2014) xxx–xxx
Contents lists available at ScienceDirect
Life Sciences
journal homepage: www.elsevier.com/locate/lifescie

Minireview

Gap junctional regulation of pressure, fluid force, and electrical fields in the epigenetics of cardiac morphogenesis and remodeling

Akiko Seki [a,b,*,1], Kiyomasa Nishii [c,1], Nobuhisa Hagiwara [a]

[a] Department of Cardiology, Tokyo Women's Medical University, 8-1 Kawada-cho, Shinjuku-ku, Tokyo 162-8666, Japan
[b] Support Center for Women Health Care Professionals and Researchers, Tokyo Women's Medical University, 8-1 Kawada-cho, Shinjuku-ku, Tokyo 162-8666, Japan
[c] Department of Anatomy and Neurobiology, National Defense Medical College, 3-2 Namiki, Tokorozawa, Saitama 359-8513, Japan

ARTICLE INFO

Article history:
Received 15 August 2014
Accepted 29 October 2014
Available online xxxx

Keywords:
Gap junction
Heart
Morphogenesis
Remodeling

ABSTRACT

Epigenetic factors of pressure load, fluid force, and electrical fields that occur during cardiac contraction affect cardiac development, morphology, function, and pathogenesis. These factors are orchestrated by intercellular communication mediated by gap junctions, which synchronize action potentials and second messengers. Misregulation of the gap junction protein connexin (Cx) alters cardiogenesis, and can be a pathogenic factor causing cardiac conduction disturbance, fatal arrhythmia, and cardiac remodeling in disease states such as hypertension and ischemia. Changes in Cx expression can occur even when the DNA sequence of the *Cx* gene itself is unaltered. Posttranslational modifications might reduce arrhythmogenic substrates, improve cardiac function, and promote remodeling in a diseased heart. In this review, we discuss the epigenetic features of gap junctions that regulate cardiac morphology and remodeling. We further discuss potential clinical applications of current knowledge of the structure and function of gap junctions.

Contents

Introduction

The heart keeps beating throughout our life. At every moment, coordinated cycles of systole and diastole are essential for proper blood delivery to tissues. The process resembles ballooning: after inflation, the air can be released from a balloon. The shape of the balloon, however, depends on how it is inflated; the thinner part expands first, but we can choose to expand other parts of the balloon, such as the tip or base, by grasping (adding pressure to) other parts. Similarly, the shape of the heart is determined by the equilibrium between tension in the cardiac walls and blood pressure. Because the heart is a dynamic organ, moment-to-moment changes of local force equilibrium constitute one of the principal epigenetic factors regulating heart morphology.

The gap junction apparatus is highly conserved in multicellular organisms, regulating coordinated contractions; i.e. the moment-to-moment changes of local force equilibrium in the heart. Mutations in

* Corresponding author at: Department of Cardiology, Support Center for Women Health Care Professionals and Researchers, Tokyo Women's Medical University, 8-1 Kawada-cho, Shinjuku-ku, Tokyo 162-8666, Japan. Tel.: +81 3 3353 8111.
E-mail address: akikokub@hotmail.com (A. Seki).
[1] These authors contributed equally to this work.

http://dx.doi.org/10.1016/j.lfs.2014.10.022
0024-3205/

Please cite this article as: A. Seki, et al., Gap junctional regulation of pressure, fluid force, and electrical fields in the epigenetics of cardiac morphogenesis and remodeling, Life Sci (2014), http://dx.doi.org/10.1016/j.lfs.2014.10.022

gap junction-encoding *connexin* (*Cx*) genes influence cardiac differentiation, morphology, and function, although the mechanisms underlying these abnormalities are not fully understood [78]. Recent advancements in mouse and zebrafish genetic models suggest that electrical fields are as important as local force equilibria; both epigenetic factors are regulated by gap junctions. Moreover, there is growing evidence that epigenetic modulation of gap junctional regulation is critical for successful recovery from compromising heart events.

Effects of fluid and electrical forces on cardiac morphology

Spontaneous, rhythmic, and coordinated action potentials of cardiomyocytes periodically alter cardiac chamber morphology. The resultant tension and fluid forces within the heart have long been assumed to be essential epigenetic morphogenic factors underlying cardiac development [73,108–110]. There is a certain class of genes whose primary function is to affect cardiac contractility rather than regulate cardiovascular morphogenesis [29]. Mutations in these genes often cause secondary cardiovascular morphogenic defects (Fig. 1a). Null mutations of *TNNT2*, encoding the thin filament contractile protein cardiac troponin T (cTnT), lead to contractile inactivity and secondary endocardial cushion defects in the developing zebrafish heart [4,95]. *cTnT*-deficient mice show dilated cardiac chambers and an endocardial cushion defect, as well as defective sarcomere assembly, which leads to a lack of heartbeats [76]. Loss of the Na^+/Ca^{2+} exchanger also causes cardiac inactivity and morphogenic defects similar to those in *cTnT*-deficient mice [12,53,90,115]. In addition to the complete lack of heartbeat, and accordingly, no blood flow, an atrium-specific contractility defect in zebrafish and mice also has a profound impact on total cardiovascular development [7,40]. These genetic models clearly show that normal blood flow and intracardiac fluid forces are essential regulators of early cardiogenesis in mammalian embryos, whose nutrient and oxygen supplies completely depend on the placenta, and in the embryos of lower vertebrates, which can be fed partly by diffusion of the extra-embryonic fluid. When blood flow within the heart is directly eliminated by surgical placement of a bead at either the inflow or outflow tracts, zebrafish hearts show an abnormal third chamber, diminished looping, and impaired valve formation [39]. Fluid force is sensed by the endothelium [73,109,110]; monocilia in the endothelial lining of the developing heart may participate in the fluid force transduction cascade [105,114]. A recent study showed flow-dependent expression of *miR-21* within the atrioventricular canal endocardium, where it regulates valve formation in zebrafish [3]. In contrast, mice lacking *miR-21* show normal cardiovascular development [84]. The precise mechanisms by which fluid

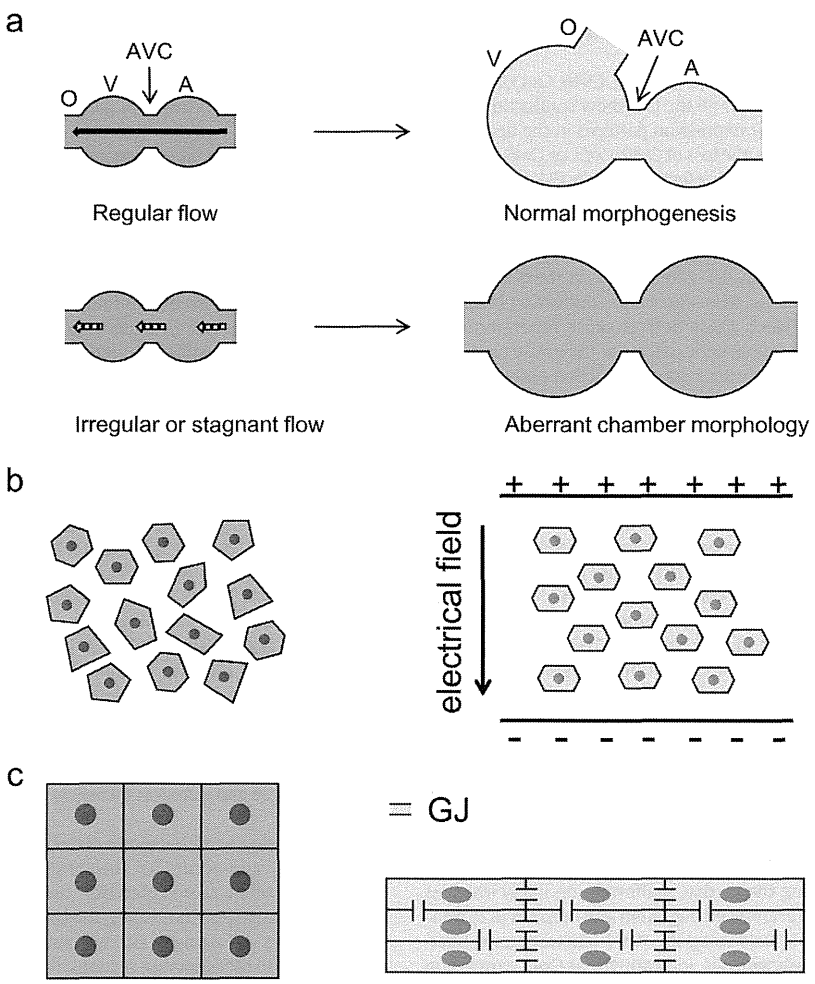

Fig. 1. Fluid force and electrical field control cardiogenesis. A, atrium; AVC, atrioventricular canal; V, ventricle; O, outflow tract.

Please cite this article as: A. Seki, et al., Gap junctional regulation of pressure, fluid force, and electrical fields in the epigenetics of cardiac morphogenesis and remodeling, Life Sci (2014), http://dx.doi.org/10.1016/j.lfs.2014.10.022

force is transduced into endothelial reactions are still largely unknown, and signaling cascades connecting fluid force, gene expression, and morphogenesis remain unexplored [25,36].

Natural electrical fields occur inside or across cells and are hypothesized to influence various biological phenomena such as cleavage furrow formation, neurite elongation, and tissue regeneration [42]. The direction of cell growth and orientation is also influenced by externally applied electrical fields, leading to cytoskeletal alterations (Fig. 1b) [63]. Theoretical consideration of cytoplasmic or intercellular electrical fields is dictated by Ohm's law: $E = IR$, where E is field strength, I is current density, and R is resistivity. A gap junction reduces intercellular resistance, thereby facilitating ionic flow between cells. A recent zebrafish study examined whether electrical control by gap junctions is sufficient to direct in vivo organogenesis (Fig. 1c) [11]. In the developing zebrafish heart, gap junction protein Cx46 is expressed in the cardiac conduction system, and the null mutant exhibits asynchronous contraction of the ventricular chamber, resulting in disorganized chamber walls. Even in the *cTnT*-deficient genetic background, where hemodynamic flow or cardiac contraction does not exist, *Cx46*-deficient zebrafish cardiomyocytes are morphologically divergent from the control cardiomyocytes. Changes in cardiomyocyte shape underlie the formation of characteristic chamber curvatures [2]. Chi et al. [11] demonstrated that physiological electrical currents through gap junctions affect cardiomyocyte cytoarchitecture and cardiogenesis.

Gap junctional control of mammalian cardiogenesis

Mouse cardiomyocytes express Cx30, Cx30.2, Cx40, Cx43, Cx45, and Cx46 [11,30,57,75]. Null strains for all the Cxs show conduction abnormalities closely related to their expression patterns in the heart [5,30, 47,56,59,89,102]. Among these, the loss of *Cx40*, *Cx43*, or *Cx45* manifests as cardiovascular developmental defects in utero [31,46,59,89,93]. These Cxs are involved in embryonic impulse propagation through cardiomyocytes, and the null mice are likely susceptible to intracardiac fluid force alterations. Cx45 is the first Cx expressed in the developing heart, around embryonic day (E) 8.5, when the heart starts beating [1] . *Cx45*-deficient embryos show atrioventricular conduction block and an endocardial cushion defect; these defects cause regurgitation of blood flow, resulting in morphogenetic defects of the entire cardiovascular system [54,59,74]. Multiple accessory conduction pathways exist within heterogeneous cardiomyocytes, consisting of *Cx45*-expressing and *Cx45*-negative cells. A subtle alteration in the distribution of *Cx45*-expressing cardiomyocytes leads to a multitude of embryonic heart shapes (unpublished) [74]. This result strongly suggests that impaired fluid force and electrical control principally lead to aberrant cardiogenesis in the *Cx45*-deficient heart. Expression of Cx40 and Cx43 starts around E9.5, when the entire primitive ventricle begins to contract almost simultaneously, replacing former peristaltic contractions, likely due to the emerging conduction system [75,77]. Bundle branch dysfunctions in *Cx40*-deficient embryos appear around E14.5 and become more prominent in later stages [47,93,102]. Consistent with conduction anomalies, *Cx40*-deficient hearts exhibit a high rate of cardiac malformations such as atrial/ventricular septal defect, double-outlet right ventricle, and endocardial cushion defect [31,46]. The molecular mechanisms by which *Cx40* deficiency leads to cardiac malformations are unknown. Whether fluid force, electrical controls, or both are involved in the malformations merits further investigation. Cx43 is the most abundant gap junction protein in the adult heart, and its absence causes swelling and blockage of the right ventricular outflow tract, as well as reduced ventricular conduction velocity [5,19,32,89]. The mechanism underlying the cardiac malformation likely involves modulation of cardiac neural crest cell migration and function [62]. Neural crest-specific deletion of *Cx43* using the *Wnt1–Cre* transgene, however, does not hamper cardiogenesis, indicating that *Cx43* expression in neural crest cells alone is not critical for proper outflow tract remodeling [55]. The involvement of conduction delay among *Cx43*-deficient ventricular cardiomyocytes in cardiac malformation has not been formally tested. Cardiomyocytes in a compromised status such as heart failure and myocardial infarction have down-regulated *Cx43* expression but upregulated *Cx40* and *Cx45* expression [68,72,80,97,98,116,120]. This Cx expression pattern is similar to that observed in the developing heart. As in normal cardiogenesis, directing proper gap junction control is important in correcting tissue remodeling and facilitating functional restoration.

Structure and gating of gap junction channels

Gap junctions allow the passage of molecules such as ions, metabolites, nucleotides, and small peptides between cells [60]. A gap junction is formed by the oligomerization of 12 Cxs. Each hexamer of a Cx (a connexon or hemichannel) docks with another in an intercalated disk between neighboring cells (Fig. 2). A connexon has its own regulatory functions in water uptake, ATP release, etc. [28]. Each Cx has four transmembrane domains (TM1–4), two extracellular loops (E1 and E2), and amino and carboxyl termini (NT and CT, respectively) at the intracellular sites. TM2 and TM3 are linked by an intracellular loop (cytoplasmic loop; CL) (Fig. 2a) [122]. Which transmembrane domain lines the pore is debated. Some reports suggest TM3 has this role (Cx43, Cx32) [24,103,112], while others report TM1 to be lining the pore (Cx32, Cx43, Cx46) [58,81,126]. The inner diameter of the channel is approximately 40 Å at the channel entrance, narrowing to 14–15 Å around the midpoint of the membrane region in Cx26 and Cx43 channels [65,112].

The opening and closing of gap junctions are regulated by various factors. There are two distinctive gating mechanisms of gap junctions, namely, transjunctional voltage and chemical gating [9]. Chemical gating operation is based on intracellular pH, Ca^{2+}/calmodulin [9,79,85], phosphorylation [106], insulin/insulin-like growth factor [38], alkanols [13,27,33], arachidonic acid [117], and volatile anesthetics [10]. Cx26 channel closing was modeled as a subunit rotation model [113]. Later, Delmar's laboratory showed that CT of Cx43 acts as a gating particle to plug the channel pore by binding the receptor in the same Cx43 CL region [20,69]. A short peptide sequence L2, named after the second half of CL, is responsible for binding (Fig. 2), which is based on the ball-and-chain model of voltage-dependent *N*-type inactivation of Shaker and other K^+ channels [6,50,124]. Recent NMR studies showed that at low pH, the binding between CT and L2 gets stronger, and CT dimerizes [17,107]. This indicates that a pH-dependent change of high-order structure between the CT and L2 affects conformation and closes the gate of the Cx43 channels. The CT region has a binding site for the desmosomal protein zonula occludens-1 (ZO-1) [111]. ZO-1 is a scaffolding protein that stabilizes Cx43 in the intercalated disk. Inhibition of the interaction between Cx43CT and ZO-1 results in internalization of Cx43 [111]. ZO-1 and Cx43 dissociate at low pH due to pH-dependent binding between tyrosine kinase c-Src and ZO-1, resulting in internalization of Cx43 [16]. ZO-1 actively constrains gap junction size by regulating the rate of channel accretion. This control mechanism, with fast turnover rates, may allow cells to respond quickly to environmental changes [41].

Remodeling of gap junction channels in a diseased heart

The changing expression and distribution of gap junctions is called "remodeling" and occurs because of pressure overload and acidosis. Remodeling often causes electrical conduction disturbance and cell morphology changes. Conversely, the correction of gap junction remodeling reverses cell damage and normalizes electrical conduction and morphology. In the following sections, the involvement of gap junctions in acute myocardial infarction; cardiac hypertrophy, including hypertrophic cardiomyopathy; and heart failure is discussed.

Please cite this article as: A. Seki, et al., Gap junctional regulation of pressure, fluid force, and electrical fields in the epigenetics of cardiac morphogenesis and remodeling, Life Sci (2014), http://dx.doi.org/10.1016/j.lfs.2014.10.022

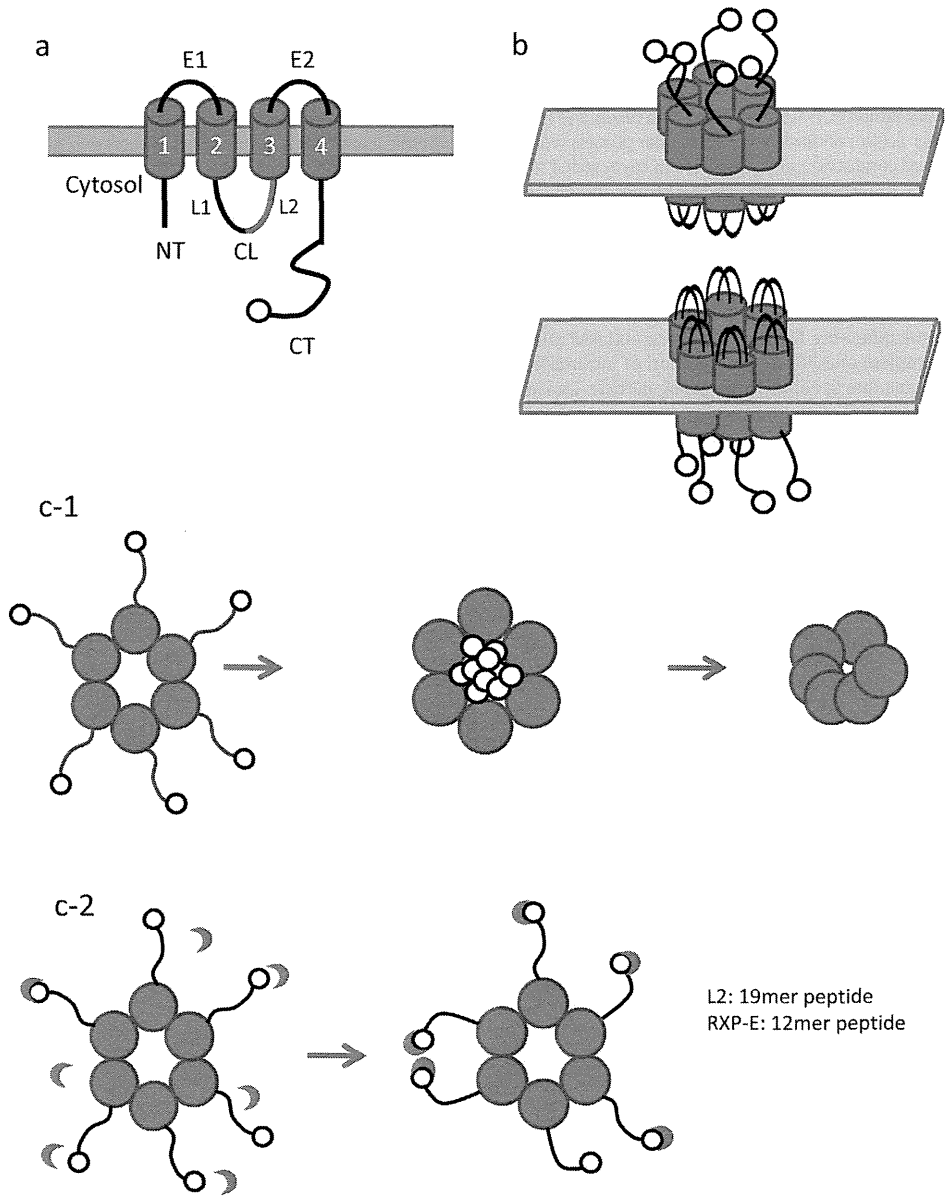

Fig. 2. Gap junction structure and gating. (a) Structure of a Cx43 molecule. The carboxyl terminal (CT) has binding domains with molecular partners such as PKA, PKC, cSrc, and ZO-1. (b) Structure of a gap junction channel. Two connexons (hexamer of Cxs) dock at a cell–cell junction. (c-1) Gap junction channels close under acidic conditions. Each blue circle corresponds to a Cx. Each Cx has six domains at the CT, but they are drawn together in one yellow ball in this figure for simplicity. Acidification makes the ball bind to its intramolecular receptor (the second half of the CL, L2) and plug the pore. Following this conformational change, the channel is completely closed. (c-2) Effect of L2 and RXP-E peptides. These peptides (red crescent) bind to the CT of Cx43 and competitively inhibit CT–L2 interaction. Accordingly, the channel does not close even in an acidic environment. 1–4, transmembrane domains 1–4; NT, amino terminal; CT, carboxyl terminal; E1 and E2, extraloops 1 and 2; CL, cytoplasmic loop; L1 and L2, the first and second halves of the CL.

Acute myocardial infarction

Ischemia depresses both electrical and chemical gap junctional communication (GJC), which causes ventricular arrhythmia and remodeling (changes in ventricle size, shape, structure, and physiology) [71,88]. Uncoupling of electrical GJC causes fatal arrhythmia, which is the main cause of sudden death in the first 1 h after myocardial infarction onset. Chemical GJC uncoupling in myocardial ischemia is said to reduce ventricular remodeling. The gap junction mediates the transfer of "death signals", such as Ca^{2+} overload, diffusion of toxic metabolites, and apoptosis signals, which increase infarct size in reperfused rat heart [27,91]. Reduced infarct size due to blockade of Cx43 hemichannels is consistent with this hypothesis [35]. Reduction in GJC, however, has significant shortcomings as a treatment for myocardial infarction. Acidification in myocardial infarction leads to closure of Cx43 channels, thereby slowing and blocking cardiac conduction in the functional myocardium, which generates a focus of reentrant ventricular tachycardia [86]. Two types of synthetic peptides can be good candidates in treating fatal arrhythmia in myocardial infarction. One (L2; RXP-E peptide) competitively inhibits intramolecular interaction to prevent pH gating of

Please cite this article as: A. Seki, et al., Gap junctional regulation of pressure, fluid force, and electrical fields in the epigenetics of cardiac morphogenesis and remodeling, Life Sci (2014), http://dx.doi.org/10.1016/j.lfs.2014.10.022

gap junction channels [96,99] (Fig. 2c) and the other (AAP; antiarrhythmic peptide), discovered in the bovine atrium, and its analogs (AAP10, ZP123, GAP134, ZP1609) enhance GJC via activation of protein kinase Cε (PKCε) [14,34,37,49,100,104,119] (Fig. 3). L2 or RXP-E binds to the CT and competitively inhibits CT–L2 interaction. As a result, the channel does not close under acidic conditions. The molecular process would be expected to improve conduction abnormalities in myocardial infarction; however, these abnormalities worsen in a mouse model lacking the Cx43 pH gating mechanism (K258stop) [64]. In K258stop mice, the incidence rate of fatal arrhythmia was significantly higher and infarct size significantly increased in a coronary ligation model. In contrast, AAP and its analogs have an antiarrhythmic effect against inducible ventricular arrhythmia and reduce infarct size [14,34,37,49,100, 104,119]. What is the difference between K258stop and AAP analogs? The former is a complete and life-long disruption of intramolecular interactions that occurs due to cutoff of the gating particle. Lacking CT in K258stop also means loss of physiologically important sites such as serine residues required for phosphorylation and the binding domains for regulatory proteins (PDZ-domain to ZO-1, etc.). Hemichannels in K258stop mice are likely to be similarly affected. AAP and its analogs, however, enhance Cx43 phosphorylation without inhibiting L2–CT interaction [15,118].

Gap junction remodeling at the infarct border zone is another arrhythmic substrate after myocardial infarction [121]. In addition to AAP analogs, αCT1 peptide, a Cx43 CT mimetic, increases phosphorylated Cx43 in vitro in a PKC-dependent manner in cryo-injured heart [82]. In the injury border zone, phosphorylated Cx43 stays in the intercalated disk and reduces inducible ventricular arrhythmia [82].

Treatment for myocardial infarction involves the contrasting approaches of chemical uncoupling and delay of electrical uncoupling. Ischemic preconditioning (IPC)—brief ischemia before subsequent ischemic events—is a natural cardioprotective mechanism that reduces arrhythmia and infarct size [70]. In IPC, activated PKC phosphorylates Cx43 and facilitates chemical uncoupling, but it also increases gap junction permeability and maintains Cx43 at the intercalated disk [21,94]. PKCε activated by AAP analogs and αCT1 seems to simulate the paradoxical effects of IPC: it attenuates electrical uncoupling (prevents arrhythmia) and facilitates subsequent chemical uncoupling (reduces infarct size) [14,82]. Revascularization therapy is not recommended for patients with advanced age, renal impairment, and other complications. In such cases, modification of gap junction channel and hemichannel function by oral or intravenous administration of AAPs will be beneficial.

Cardiac hypertrophy and hypertrophic cardiomyopathy

Mechanical stress, such as that in hypertension, causes cardiac hypertrophy when gap junctions are upregulated in human and animal models [51]. Exposure of cultured ventricular cardiomyocytes to a membrane-permeable form of cAMP, angiotensin II, and vascular endothelial growth factor upregulates Cx43 gap junction [92]. In the early stages of hypertrophy, this results in faster electrical conduction

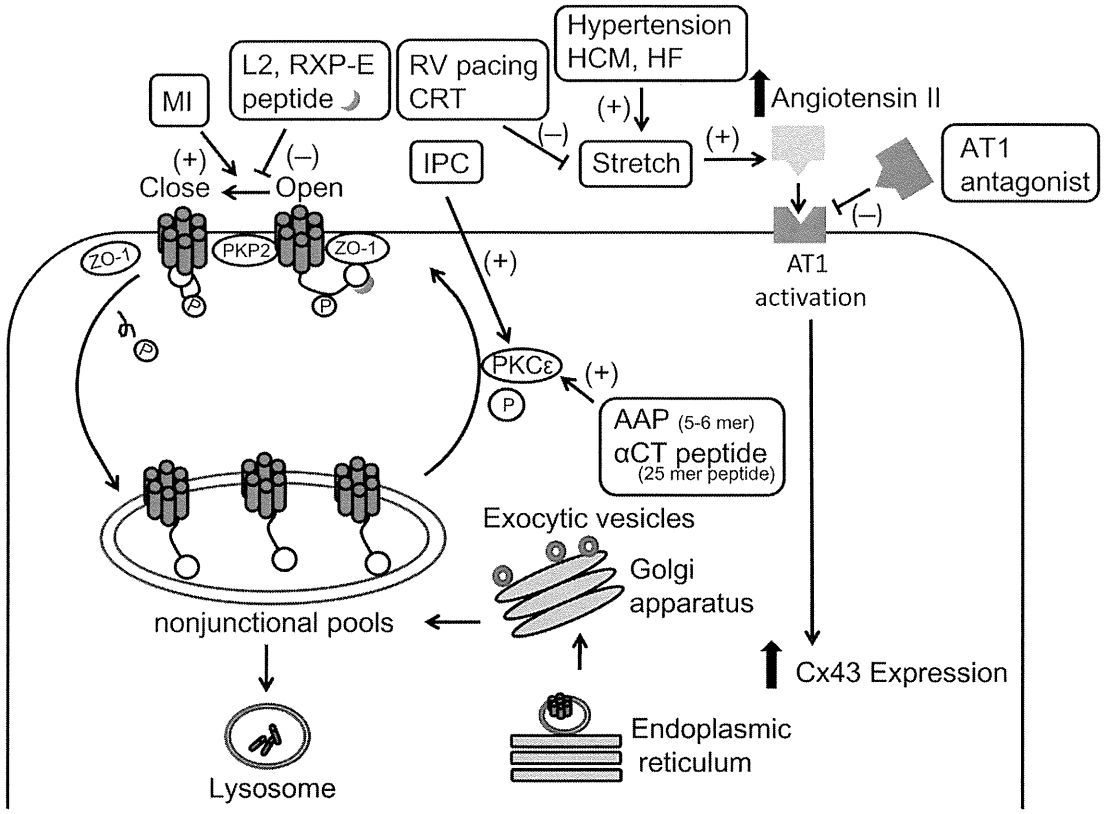

Fig. 3. Expression, modulation, and degradation of gap junctions. Mechanical force (stretch), ischemia (MI, myocardial infarction; IPC, ischemic preconditioning), and heart failure (HF) change the expression and distribution of Cxs in the myocardium. These changes can be reversed by epigenetic tools that reduce mechanical force and correct electrical conduction. AAP, antiarrhythmic peptide; HCM, hypertrophic cardiomyopathy; RV pacing, right ventricular pacing; CRT, cardiac resynchronization therapy; PKCε, phosphokinase Cε; AT1, angiotensin II receptor 1; ZO-1, zonula occludens 1; PKP2, plakophilin-2.

Please cite this article as: A. Seki, et al., Gap junctional regulation of pressure, fluid force, and electrical fields in the epigenetics of cardiac morphogenesis and remodeling, Life Sci (2014), http://dx.doi.org/10.1016/j.lfs.2014.10.022

velocity. Antihypertensive drug angiotensin II type 1 receptor (AT1) antagonists normalize Cx43 expression, thereby reversing the symptoms of cardiac hypertrophy [22,101,123].

Hypertrophic obstructive cardiomyopathy (HOCM) is characterized by asymmetric left ventricle hypertrophy and outflow tract obstruction with a >30 mm Hg pressure gradient between the left ventricle and outflow tract (LVOTPG) [67,83]. LVOTPG sometimes reaches >100 mm Hg, which causes syncope and sudden death. Other than ventricular septal myectomy and pacemaker therapy, Na^+ channel blockers have been used to reduce LVOTPG in HOCM [45]. Na^+ channel complexes at intercalated disks are in close association with N-cadherin and Cx43 [66]. Cx43 alone is insufficient; both Cx43 and Nav1.5 (α subunit of the Na^+ channel complex) are necessary for cell-to-cell transmission of action potential [32,43,61]. Accordingly, treatment with Na^+ channel blockers likely involves a decrease in GJC. Under ventricular pacing—an alternative to surgery—the normal cardiac conduction system is bypassed by preexcitation of the right ventricular apex, thereby reducing paradoxical movement of the interventricular septum and outflow obstruction [23]. The improvement of LVOTPG and other cardiac functions after pacing indicates that ventricular remodeling in cardiac hypertrophy can be reversed by reducing mechanical force and applying electrical stimulation.

Heart failure and ventricular remodeling

Cx43 is markedly downregulated in the left ventricle in human end-stage heart failure due to ischemic cardiomyopathy, idiopathic dilated cardiomyopathy [18], decompensated cardiac hypertrophy [51], and myocarditis [52]. In the failing heart, Cx43 expression is decreased and disorganized [87]. Although the precise molecular mechanisms are unclear, ZO-1 is upregulated in parallel with Cx43 downregulation [8]. In the failing heart, conduction slows due to gap junction remodeling, causing fatal arrhythmia and sudden death. AT1 blockade modulates adherens and gap junction remodeling, and has been postulated as a new therapy for fatal ventricular arrhythmia [123]. Recently, a mutation in plakophilin-2 (PKP2) was reported in familial arrhythmogenic right ventricular cardiomyopathy [44]. Since PKP2, a desmosomal protein, interacts with Cx43, mutated PKP2 downregulates Cx43. AAP analogs and αCT peptide may be effective in treating this disease because they stabilize Cx43 in the membrane and improve arrhythmia in the failing heart.

Marked fibrosis and dilation of the ventricles are observed in some severe cases of heart failure. Surface ECG sometimes shows a wide QRS complex rhythm and atrioventricular conduction block. Cardiac resynchronization therapy is the course chosen for such patients [26]. Similar to HOCM, correction of electrical conduction is important for reversing ventricular remodeling in the failing heart.

Conclusion

In this review, we discussed gap junction epigenetics in heart development, morphogenesis, and disease. Peptide therapy is a promising new approach that can be used instead of or combined with drug therapy. Clinical trials of peptides ZP123 and GAP134 have been underway since 2004 [48,125]. Reduction of mechanical forces and correction of electrical conduction involves alterations of gap junction and other signaling pathways, thereby reversing remodeling of the hypertrophic failing heart. In myocardial infarction, peptides that not only increase the permeability of gap junctions but also facilitate chemical uncoupling are expected to reduce arrhythmia and necrosis. Control of gap junctions and hemichannels suppresses arrhythmogenesis and reduces remodeling in diseased myocardium. Modifying interactions among Cxs and adhesion/desmosomal proteins such as N-cadherin, β-catenin, ZO-1, and PKP2 may reduce gap junction remodeling. Gap junction-targeted therapy does not simply "open" or "close" channels but controls the quantity, permeability, distribution, and timing of GJC. Combined therapy of several gap junction-targeted drugs might improve clinical outcomes in the treatment of heart diseases.

Conflict of interest statement

The authors declare that there are no conflicts of interest.

Acknowledgments

This work was supported by Grants-in-Aid for Scientific Research from the Japan Society for the Promotion of Science [grant numbers 23591091 to A.S., 22590197 to K.N.], and the Takako Satake Research grant for Support Center for Women Health Care Professionals and Researchers to A.S.

References

[1] S. Alcoléa, M. Théveniau-Ruissy, T. Jarry-Guichard, I. Marics, E. Tzouanacou, J.P. Chauvin, J.P. Briand, A.F. Moorman, W.H. Lamers, D.B. Gros, Downregulation of connexin 45 gene products during mouse heart development, Circ. Res. 84 (1999) 1365–1379.
[2] H.J. Auman, H. Coleman, H.E. Riley, F. Olale, H.J. Tsai, D. Yelon, Functional modulation of cardiac form through regionally confined cell shape changes, PLoS Biol. 5 (2007) e53.
[3] T. Banjo, J. Grajcarek, D. Yoshino, H. Osada, K.Y. Miyasaka, Y.S. Kida, Y. Ueki, K. Nagayama, K. Kawakami, T. Matsumoto, M. Sato, T. Ogura, Haemodynamically dependent valvulogenesis of zebrafish heart is mediated by flow-dependent expression of miR-21, Nat. Commun. 4 (2013) 1978.
[4] T. Bartman, E.C. Walsh, K.K. Wen, M. McKane, J. Ren, J. Alexander, P.A. Rubenstein, D.Y. Stainier, Early myocardial function affects endocardial cushion development in zebrafish, PLoS Biol. 2 (2004) E129.
[5] P. Beauchamp, C. Choby, T. Desplantez, K. de Peyer, K. Green, K.A. Yamada, R. Weingart, J.E. Saffitz, A.G. Kléber, Electrical propagation in synthetic ventricular myocyte strands from germline connexin43 knockout mice, Circ. Res. 95 (2004) 170–178.
[6] D. Bentrop, M. Beyermann, R. Wissmann, B. Fakler, NMR structure of the "ball-and-chain" domain of KCNMB2, the beta 2-subunit of large conductance Ca^{2+}- and voltage-activated potassium channels, J. Biol. Chem. 276 (2001) 42116–42121.
[7] E. Berdougo, H. Coleman, D.H. Lee, D.Y.R. Stainier, D. Yelon, Mutation of weak atrium/atrial myosin heavy chain disrupts atrial function and influences ventricular morphogenesis in zebrafish, Development 130 (2003) 6121–6129.
[8] A.F. Bruce, S. Rothery, E. Dupont, N.J. Severs, Gap junction remodelling in human heart failure is associated with increased interaction of connexin43 with ZO-1, Cardiovasc. Res. 77 (2008) 757–765.
[9] F.F. Bukauskas, C. Peracchia, Two distinct gating mechanisms in gap junction channels: CO_2-sensitive and voltage-sensitive, Biophys. J. 72 (1997) 2137–2142.
[10] J.M. Burt, D.C. Spray, Volatile anesthetics block intercellular communication between neonatal rat myocardial cells, Circ. Res. 65 (1989) 829–837.
[11] N.C. Chi, M. Bussen, K. Brand-Arzamendi, C. Ding, J.E. Olgin, R.M. Shaw, G.R. Martin, D.Y.R. Stainier, Cardiac conduction is required to preserve cardiac chamber morphology, Proc. Natl. Acad. Sci. U. S. A. 107 (2010) 14662–14667.
[12] C.H. Cho, S.S. Kim, M.J. Jeong, C.O. Lee, H.S. Shin, The Na^+–Ca^{2+} exchanger is essential for embryonic heart development in mice, Mol. Cells 10 (2000) 712–722.
[13] G.J. Christ, M. Spektor, P.R. Brink, L. Barr, Further evidence for the selective disruption of intercellular communication by heptanol, Am. J. Physiol. 276 (1999) H1911–H1917.
[14] S. Dhein, Peptides acting at gap junctions, Peptides 23 (2002) 1701–1709.
[15] S. Dhein, B.D. Larsen, J.S. Petersen, F.W. Mohr, Effects of the new antiarrhythmic peptide ZP123 on epicardial activation and repolarization pattern, Cell Commun. Adhes. 10 (2003) 371–378.
[16] H.S. Duffy, A.W. Ashton, P. O'Donnell, W. Coombs, S.M. Taffet, M. Delmar, D.C. Spray, Regulation of connexin43 protein complexes by intracellular acidification, Circ. Res. 94 (2004) 215–222.
[17] H.S. Duffy, P.L. Sorgen, M.E. Girvin, P. O'Donnell, W. Coombs, S.M. Taffet, M. Delmar, D.C. Spray, pH-dependent intramolecular binding and structure involving Cx43 cytoplasmic domains, J. Biol. Chem. 277 (2002) 36706–36714.
[18] E. Dupont, T. Matsushita, R.A. Kaba, C. Vozzi, S.R. Coppen, N. Khan, R. Kaprielian, M.H. Yacoub, N.J. Severs, Altered connexin expression in human congestive heart failure, J. Mol. Cell. Cardiol. 33 (2001) 359–371.
[19] D. Eckardt, M. Theis, J. Degen, T. Ott, H.V.M. van Rijen, S. Kirchhoff, J.S. Kim, J.M.T. de Bakker, K. Willecke, Functional role of connexin43 gap junction channels in adult mouse heart assessed by inducible gene deletion, J. Mol. Cell. Cardiol. 36 (2004) 101–110.
[20] J.F. Ek-Vitorin, G. Calero, G.E. Morley, W. Coombs, S.M. Taffet, M. Delmar, PH regulation of connexin43: molecular analysis of the gating particle, Biophys. J. 71 (1996) 1273–1284.
[21] J.F. Ek-Vitorin, T.J. King, N.S. Heyman, P.D. Lampe, J.M. Burt, Selectivity of connexin 43 channels is regulated through protein kinase C-dependent phosphorylation, Circ. Res. 98 (2006) 1498–1505.
[22] L. Emdad, M. Uzzaman, Y. Takagishi, H. Honjo, T. Uchida, N.J. Severs, I. Kodama, Y. Murata, Gap junction remodeling in hypertrophied left ventricles of aortic-banded

Please cite this article as: A. Seki, et al., Gap junctional regulation of pressure, fluid force, and electrical fields in the epigenetics of cardiac morphogenesis and remodeling, Life Sci (2014), http://dx.doi.org/10.1016/j.lfs.2014.10.022